PREPARATION FOR NOVEL ISOTOPE HARVESTING METHODS AND CHEMISTRY FOR USER BEAM DEVELOPMENT

By

Andrew C. Candia

A THESIS

Submitted to
Michigan State University
in partial fulfillment of the requirements
for the degree of

Chemistry – Master of Science

2024

ABSTRACT

At the Facility for Rare Isotope Beams (FRIB), development has been underway to collect radionuclides that are produced as by-products of dumping the unused portion of the primary beam into a flowing-water beam stop. This technique, known as 'isotope harvesting,' has been tested in several exploratory studies and demonstrated its capability to collect isotopes from the water system. Isotope harvesting is predicted to be a promising source of isotopes, essential for advancing both basic and applied sciences. However, this method is inherently non-selective, and most isotopes can only be recovered from the water at limited radioisotopic purity. A viable method to improve the purity of the harvested samples is by implementing a mass-separation step.

Metal oxides were proposed as potential novel sorbent materials, as their refractory nature makes them compatible with the high-temperature environment of the plasma ion source of the mass separator, a feature that makes the envisioned combined approach possible. In the here-performed research, the feasibility of using metal oxides for isotope collection has been investigated. Simulation studies have been performed with nickel, which represents our main isotopes of interest, and nine other stable elements that are the main co-produced isotopes, under conditions similar to the predicted harvesting environment in the aqueous beam dump. Several of the tested metal oxides demonstrated adequate adsorption abilities for certain elements, while magnesium oxide emerged as the most promising for Ni capture. This was used to produce a sample of magnesium oxide with adsorbed, stable, enriched ^{61}Ni for a proof-of-principle mass-separation experiment. The results showed that mass separation performance with oxide-based samples is highly challenging due to the formation of various, partially refractory, species. In retrospect, it was also observed that the use of certain metal oxides, particularly magnesium oxide, results in the release of ions into the aqueous environment, which is undesirable. Based on these findings, while the insoluble metal oxides could see applications for the adsorption of particular elements, it was decided to consider different targetry options for the mass-separation step.

In the second part of this work, research was also done to develop a ^{73}As source material for the low-energy and stopped user beam program at FRIB. The source sample was prepared through precipitation of aqueous ^{73}As, after addition of stable As carrier, as silver arsenate. The ^{73}As source was submitted and used to successfully create a ^{73}As beam. Characterization via Scanning Electron Microscopy-Energy Dispersive X-Ray (SEM-EDS) and X-Ray Photoelectron Spectroscopy (XPS) was done with an analogously prepared stable As source sample.

ACKNOWLEDGMENTS

I want to spend some time acknowledging the many people who all deserve my thanks and praise. I first want to give special thanks to my advisor, Dr. Katharina Domnanich, who welcomed me to her group during a time when my future was uncertain at Michigan State University. I know that things were never easy, especially with me, but I am forever grateful that I got the chance to work with such a capable and successful scientist as yourself. From transitioning lab groups to helping me decide my academic future, you helped me every step of the way. I want to also thank your patience, as I know there were times I struggled to meet expectations, I am so happy to have been through this journey with you. Truly, thank you Kathi. I want to also thank each member of my committee: Dr. Alyssa Gaiser, Dr. Sean Liddick, Dr. Gregory Severin, and Dr. Kyle Brown, for your patience and support in guiding my academic future beyond MSU. I want to thank the other scientists and people I got to meet while here at MSU. Specifically, for the folks with BMIS, Dr. Chandana Sumithrarachchi, Christopher Izzo, and Nadeesha Gamage, and the scientists with ISOLDE, thank you for giving me the research opportunities at FRIB, and wish the best in your future work toward isotopes and isotope harvesting. Thanks as well to Abigail Vanderberg and Per Askeland for your help with all my source sample work. Thank you, Dr. Weiwei and Jose Jimenez Gonzalez, for providing me with the materials and needed assistance to also refine my research.

I also want to thank some peer researchers from these groups. As a whole, I want to just thank you all for sitting through my practice talks and giving me feedback and advice for my papers, including this thesis. Without any of you, the quality of my work would not be where it is now. First, to Deepika; although you have only joined our group I leave feeling confident knowing Kathi is with such a strong scientist and person. For all the times you helped with research, or even simple car rides and conversations, they meant a lot to me. I am so proud to call you my friend. Our summer student Suvan, your time was short, but the work you had done in just one summer has helped our research. It cannot be understated that this work would not have been possible without your contributions, and only wish the best in your future career aspirations. Finally, Kiersten; you joined recently as an undergrad, but your contribution has not gone unnoticed. I am happy to have helped you during your research and thankful for your assistance with mine. Since joining the nuclear team, I am so happy to have worked with Chloe, Vlad, and Jose; our time was always sporadic, but I am glad to have met each and every one of you. I also

want to include Chirag, Wes, and Samridhi; thank you for your time and feedback during our Friday meetings. To everyone in the Gaiser group, thank you for providing a space to always present and get help with our work, and special thanks to Nicholas, Trenton, Mike, and Michaela. I am not a good talker, so I know that we never were close, but I am still happy that the times I needed help with a presentation or paper, you all were willing to listen. It truly means a lot to me. Thank you all for getting me to where I am today.

I want to thank the friends and people I met while at MSU, for their support outside of the college, and even sometimes during it. A huge thanks to my best friend Jess, the best person anyone could ask for. We had a lot of laughs, game nights, and random Biggby runs. The memories spent while at MSU will always be with me. Thank you for being you, and staying with me throughout all of this. To all the folks, past and present, with Board Game Night, there were so many nights, days, and celebrations that I got to be a part of, so thank you all for the time spent. Thank you to Shommo and Kahini, my oldest friends, I am still so happy that you are but a text away and still a part of my life. The same for Susana, I never call as much, but we have seen each other through hard times. Thank you for still wanting to be a part of my life.

I finally wish to thank all my family and loved ones. To my mom, Kimberly, and dad, Gabriel, you always were a phone call away, and were always there during the best and worst of me. Words alone cannot express what you mean to me, and how I am only where I am today through you both. For Abuela and Abuelo, there is always love and comfort, the chances I get to see you both were always the best knowing I got to be with you. For Uncle Michael and Nataly, the same is true with you, where when we were all together, there was never a shortage of love. To my sisters, Kaylee and Danielle, and my brother Darren, the fun days and game sessions we all had are not lost to me and I love you all. To Reggie, my brothers Julian and JP, Titi Desi, Grandma Gladys, and all the other folks from my other family, while our time is always so short and I wish we were still together like before, I am still happy that you are all a part of my life and hope that despite the challenges, you get the best because you deserve it. To everyone, mi familia, I am happy that I got to share my life with everyone.

In loving memory of my mom, Julie, I want to dedicate the rest of the thesis to you. I wish you were here to witness all that I have done, but can only hope that I continue to do you proud. You always put the family over yourself, and I hope to one day get to become the same person as you were. Miss you everyday. I love you Mom.

TABLE OF CONTENTS

CHAPTER 1: Introduction

1.1: Isotopes and Applications

The nuclear science community has consistently emphasized a growing need for non-standard radioisotopes in the U.S., as demands are surpassing the existing supply capabilities. This was underlined by the 2015 published report from the Nuclear Science Advisory Committee – Isotopes Subcommittee. The significance of radioisotopes cannot be understated: clinical treatment and pharmaceuticals utilize the energy emitted from radioisotopes as a 'tracer' to better diagnose diseases in the body and use this radiation to treat and monitor various diseases. Radioisotopes as radiotracers are also used in environmental studies, as the radiation can accurately follow the chemical and biological pathways of different ecosystems. In the leading nuclear facilities across the U.S., enriched isotopes provide beams to study nuclear structure, quantum mechanics, and other physics research. The National Nuclear Security Administration (NNSA) uses radioisotopes to detect nuclear material, and the Transportation Security Administration (TSA) uses them in detectors for regularly screening incoming cargo and airport security.[1,2] While there is a wide range of highly interesting radioisotopes, our main focus is directed towards the production of highly pure radioactive nickel isotopes.

1.2: Nickel Radioisotopes

Our research group is particularly interested in nickel isotopes. Nickel has five naturally occurring isotopes: ^{58}Ni, ^{60}Ni, ^{61}Ni, ^{62}Ni, and ^{64}Ni that see applications in nuclear physics and synthesizing various copper isotopes ($^{60, 61, 64}$Cu) that are important for applications in nuclear medicine.[3,4] The nickel radioisotopes: ^{56}Ni, ^{57}Ni, ^{59}Ni, and ^{63}Ni are relevant for a variety of disciplines, such as astrophysics research, material science, nuclear medicine, biological tracers, and national security. In nuclear astrophysics, ^{56}Ni and ^{63}Ni are highly desired target materials for reaction rate studies, which will contribute to shed light on the formation of the elements in the universe.[5] The positron-emission of ^{57}Ni shows promise as a useful radioisotope for Positron-Emission Tomography (PET) imaging, as well as a radiotracer in studying the toxicokinetics of nickel.[6,7] Both ^{59}Ni and ^{63}Ni are used as biomedical tracers, detector materials, and in cosmic radiation studies, alongside applications for astrophysics research.[8] In particular, ^{59}Ni is used to study the radiation of extraterrestrial matter, while ^{63}Ni is used in national security applications as an ionization source for explosive residue detectors and in Electron Capture Detectors (ECD) for analytical instruments, such as gas chromatographs.[9–11] During irradiation of stable ^{58}Ni inside

fusion reactors, which is a part of many structural components, the (n, γ) reaction produces ^{59}Ni that ultimately undergoes an (n, α) reaction to ^{56}Fe, releasing helium that can cause damage to the structural material of these reactors.[12,13] Researchers are therefore interested in investigating the cross-section of the ^{59}Ni (n, α) reaction, and would require ^{59}Ni source materials to perform such measurements. Considering the wide range of applications for Ni radioisotopes, there is a strong rationale for investigating methods to produce them at high radioisotopic purities.

With the promise of utilizing nickel isotopes in these disciplines, the difficulty is the generation of sufficient quantities at high radioisotopic purities. For example, radioisotopes as reaction targets in nuclear astrophysics have to be available in sizeable quantities and with sufficient radioisotopic purity to be a viable sample material, with similar requirements for nuclear medicine, biological tracers, and detectors.[14,15] Despite the wide interest in Ni isotopes, a production method that can yield the desired quantities of high-purity samples is still lacking. In the following work, one aspect of this challenge will be addressed.

1.3: FRIB and Isotope Harvesting

At the Facility for Rare Isotope Beams (FRIB), rare isotope beams are generated for nuclear physics research. FRIB consists of a super-conducting radiofrequency heavy-ion linear accelerator that is predicted to deliver beam powers of 400kW and accelerate all stable isotopes, ranging from hydrogen to ^{238}U. This accelerator will create heavy-ion primary beams that impinge on a target. Only a small percentage of the primary beam will react with the target to produce a variety of isotopes. The generated isotopes enter a dipole magnet separator that separates the isotopes and delivers the desired exotic secondary beams to scientific user experiments. The unused primary beam is usually directed into a solid beam blocker.[16–18]

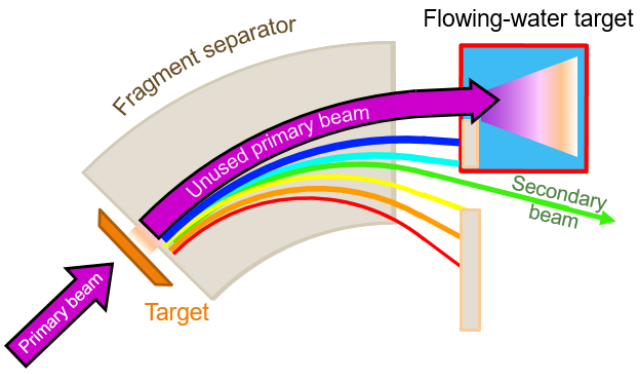

Figure 1: Schematic for Isotope Harvesting at FRIB provided by G. Severin.

By replacing the solid beam blocker with a water-filled target, a large portion of the

unused primary beam can be collected. In this process, nuclear reactions between the primary beam and the water molecules (fragmentation, spallation, fusion-evaporation) will produce a variety of radioisotopes. These species can be extracted from the water, which became known as 'isotope harvesting'. This process is visualized in Figure 1. Through isotope harvesting, exotic isotopes can be accessed, which are produced as by-products of standard accelerator operation without requiring costly irradiation time. The collection process occurs in the background and does not interfere with the usual operation of FRIB. The feasibility of isotope harvesting was demonstrated at FRIB's predecessor facility, the National Superconducting Cyclotron Laboratory (NSCL). Beams of ^{24}Na, ^{40}Ca, ^{48}Ca, ^{76}Ge, and ^{78}Kr were captured in a liquid water matrix. The generated aqueous radioisotopes were harvested from the water using ion exchange beds, while cooled stainless-steel traps were used to collect the gaseous radioisotopes. The harvested radioisotopes from these experiments encompass ^{24}Na, ^{47}Ca, ^{48}V, ^{62}Zn, ^{67}Cu, and ^{76,77}Kr.[18–26] It is notable, that the aqueous phase in the isotope harvesting setup has a neutral pH and consists of pure water that is devoid of any ions.

So far, the main focus of isotope harvesting was laid on generator isotopes – harvesting the longer-lived parent radionuclides, followed by purification, and then decay to the desired daughter isotope.[23] This approach, however, does not work efficiently with parent radionuclides that have too short half-lives. When directly harvesting the daughter radioisotope and even after performing chemical separation, the purified sample will still contain a range of isotopes of the same element. An alternative technique is required in order to broaden the spectrum of harvestable isotopes at FRIB that can be obtained at high radioisotopic purity.

1.4: Mass Separation and BMIS

Mass separation is a way to separate individual isotopes based on their mass, resulting in samples with enhanced radioisotopic purity. In an attempt to combine isotope harvesting with mass separation, the radioisotopes from the water dump system will be collected on a sorbent material, like metal oxides. Metal oxides exhibit refractory properties, which makes it possible to directly introduce the entire assembly into the high-temperature environment of the mass separator's plasma ion source. With this, the direct combination of isotope harvesting and mass separation comes into reach. For the mass separation system, the already existing infrastructure at FRIB will be used. The key elements are the Batch Mode Ion Source (BMIS), a plasma ion source (shown in Figure 2), and a magnet, which are situated on the same beamline (a more detailed

discussion of BMIS operation can be found in section 3.1.1). The introduced sample is heated, atomized, and finally ionized. The ion beam enters the mass separator that separates each isotope by mass. So far, this setup has been used to deliver offline beams to other user facilities at FRIB.[27] To run offline samples within BMIS, a source sample is prepared onto a sheet of tantalum, and deposited into the oven, shown in Figure 2.[28] Similar mass separation systems are currently in place with the Isotope Separation On-Line facilities at the European Organization for Nuclear Research (ISOLDE-CERN), as well as its Medical Isotopes facilities (CERN-MEDICIS).[29,30] For our research, we envision the collection of the separated isotopes on individual metallic foils in the future. Any co-implanted isobaric impurities and the bulk amount of matrix material can be removed via chemical separation. What remains would be the desired radioisotope with enhanced radioisotopic purity. Figure 3 outlines this projected scheme.

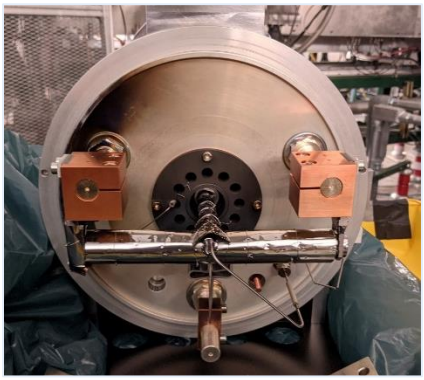

Figure 2: Image of the Batch Mode Ion Source. Image provided by K. Domnanich.

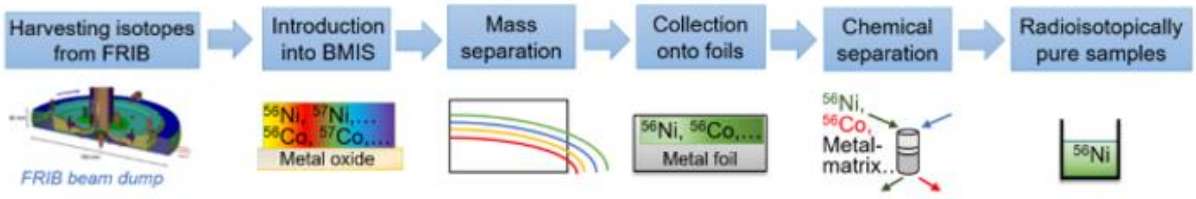

Figure 3: Flow diagram of the proposed isotope harvesting process. Radioisotopes are first produced in the aqueous phase. Metal oxides will adsorb the isotopes and the entire assembly will be directly introduced into BMIS. This will be followed by mass separation of the isotopes. The purified isotopes will then be collected onto foils and chemically separated to obtain a radioisotopically pure sample.

The BMIS is able to work at minimum temperatures of 300°C and can go as high as around 1800°C.[28] These temperatures can allow for efficient atomization of the inserted samples; however, these operating conditions require a matrix that can survive those temperatures. In the

past, isotope separation used ion exchange resins as a sorbent due to their affordability and reliable application.[31] However, most ion exchange resins would degrade under the BMIS temperature conditions. Our research group proposed the use of metal oxides as a sorbent material: their refractory nature would ensure thermal stability.[32] In addition, the metal oxides would provide a seamless combination of isotope harvesting and mass separation.

One goal of this work was to assess the adsorption capabilities of metal oxides as a potential sorbent for isotope harvesting. This was accomplished through simulation experiments with stable element samples and applying the expected isotope harvesting conditions. During the simulation with metal oxides, a collaboration was held with the BMIS researchers in the development of a source sample to allow the generation of offline beams for user experiments. This work would allow for the acquisition of the necessary expertise within our research team in assessing the necessary qualities a sample must have to perform a successful run. Herein we describe the research progress in both: the development of the mass-separation option by testing the adsorption capability of various metal oxides, as well as the efforts in the preparation of a ^{73}As source sample for BMIS operation.

CHAPTER 2: Metal Oxides

2.1: Background

Metal oxides are considered as an alternative sorbent material for isotope harvesting. Their refractory nature would make them compatible with the high temperatures inside the BMIS, and provide a direct combination of isotope harvesting and mass separation. Metal oxides have already seen use as a sorbent for wastewater treatment and water purification.[33] Researchers at ISOLDE, CERN have also demonstrated success in using metal oxides as target materials.[29] The work done then hopes to use such metal oxides for our isotope harvesting setup at FRIB. In order to assess the sorption abilities of the metal oxides, adsorption studies were done with 10 stable elements that would represent the radioisotopes of interest. Our group was especially interested in the adsorption of nickel, though the adsorption of the other elements was also investigated as those radioisotopes are also of significant scientific interest. When metal oxides come into contact with an aqueous solution, their surface becomes hydroxylated (MOH). This hydroxyl layer can be protonated or deprotonated, resulting in an electrical surface charge. This charge can dictate the species that readily adsorb to the metal oxides.[34] The overall charge on each metal oxide depends on the larger concentration of ions present, according to the equations below:

$$MOH(surf) + H_2O \rightleftharpoons MOH_2^+(surf) + OH^-(aq) \quad (2)$$

$$MOH(surf) + H_2O \rightleftharpoons MO^-(surf) + H_3O^+(aq) \quad (3)$$

The point at which the net charge of the metal oxide surface is zero is the Point of Zero Charge (PZC). The PZC of the metal oxide determines the expected surface charge at a certain pH. If the solution pH is below the PZC, the metal oxide will have a positively charged surface (MOH_2^+), and if the solution pH is above the PZC, the metal oxide has a negatively charged surface (MO^-).[34,35] By plotting the initial pH against the change in pH (ΔpH), the PZC of the metal oxide can be determined. Work had also been done to determine the PZC of each metal oxide to predict the adsorption of each element to the oxide. A large part of the resulting adsorption data and PZC data was obtained by Suvan Campbell as a part of his summer research program. It is important to note that the harvesting conditions of the water system are kept at a neutral pH, and devoid of any ions.

2.2.: Metal Oxide Characterization

The metal oxide structure was characterized via Powder X-Ray Diffraction (XRD) using a Rigaku Miniflex Powder Diffractometer. The metal oxides used in this work are listed in Table 1.

The available metal oxides were grounded, placed on a 0.2mm thick silicon rectangular sample holder, and the XRD spectra were acquired using the DIFFRAC.EVA software. The resulting spectra are compared with the references available in the Crystallographic Open Database (COD). The output consists of a list of the possible phases and the percentage match.

Table 1: Compiled list of the tested sorbent materials, including the chemical formula, reported particle size, purity, and retailer details.

Sorbent	Formula	Particle Size	Purity	Company
Zirconium (IV) Oxide	ZrO_2	5µm	99% trace metals basis	Sigma-Aldrich
Yttrium (III) Oxide	Y_2O_3	-	99.99% trace metals basis	Sigma-Aldrich
Magnesium Oxide	MgO	-325 mesh	≥99% trace metals basis	Sigma-Aldrich
Titanium (IV) Oxide	TiO_2	-	99-100.5%	Sigma-Aldrich
Cerium (IV) Oxide	CeO_2	<5µm	99.9% trace metal basis	Sigma-Aldrich
Silica Gel	SiO_2	63-200µm	High-Purity Grade	Sigma-Aldrich
Titanium Dioxide Nano-powder	TiO_2	100nm	99.9%	US Research Nanomaterials Inc.
Graphite	C	50 mesh	99.50%	ACS Material

2.3: Stock Solution Preparation

To evaluate the efficiency of metal oxide adsorption, testing was done with 10 stable elements. The 10 elements represent the isotopes that are expected to be mainly produced in the beam dump by ^{58}Ni and ^{78}Kr primary beams. Table 2 lists each element and the available ICP stock solutions. Before using these solutions for the planned experiments, the nitric acid (HNO_3) matrix was removed. Several 10mL beakers were rinsed with De-Ionized (DI) water and left briefly to incubate in 1M HNO_3. After discarding the acid, the beakers were rinsed with MilliQ water (conductivity of 18.20MΩ*cm). A volume of 3mL of each stock solution was pipetted into each beaker, placed on a few hot plates set to 120°C, and brought down to a residue. These formed

residues were reconstituted with 500µL MilliQ water. In case the residue did not dissolve in water, the mixture was heated, and if any solid remained, the solution would be treated with 350µL 70% HNO_3. This was followed by subsequent evaporation and reconstitution with MilliQ water. These reconstituted solutions were transferred into 10 pre-weighed 5mL Eppendorf tubes. The beakers were rinsed three times with a small volume of MilliQ water, and those rinses were transferred to the respective tubes and weighed.

Table 2: Reagent data for all used ICP element solutions. The data includes the concentration and error, the given matrix, and the manufacturer.

Element	Concentration (ppm)	Error (ppm)	Matrix	Company
Arsenic	997	±4	3-5% HNO_3	Sigma-Aldrich
Chromium	1000	-	3-5% HNO_3	GFS Chemicals
Cobalt	1000	±2	3-5% HNO_3	Sigma-Aldrich
Copper	1000	-	2% HNO_3	SPEX CertiPrep
Manganese	1003	±5	2% HNO_3	Sigma-Aldrich
Nickel	1000	±2	2% HNO_3	Sigma-Aldrich
Scandium	1000	±10	5% HNO_3	GFS Chemicals
Selenium	1000	±10	5% HNO_3	GFS Chemicals
Vanadium	1000	±10	5% HNO_3	GFS Chemicals
Zinc	1000	±10	5% HNO_3	GFS Chemicals

To confirm the concentrations of each element in each tube, the concentrations were quantitatively measured using an Agilent 5900 Inductively Coupled Plasma-Optical Emission Spectroscopy (ICP-OES). The reconstituted solutions were diluted by a ratio of 1:100 using 3% HNO_3 as the matrix to reach concentrations of about 10ppm. This dilution was used to make two dilutions of 1:5 and 1:10 respectively. Another set of samples was also prepared as calibration standards using each element stock solution; each ICP standard from Table 2 was diluted by a 1:5 ratio with 3% HNO_3 to reach a concentration of 200ppm. A portion of each 200ppm solution was used to make a 10ppm mixed metal standard. Portions of this mixed metal standard were used to prepare calibration standards of 1, 5, and 10ppm respectively. A 3-point calibration curve using these standards was generated and allowed to accurately determine the concentration of each present element in the reconstituted solutions.

2.4: Testing the Metal Oxide Adsorption

While the pH of the water in the isotope harvesting system will have a neutral pH, the following experiments were conducted at a pH of 5.6. This was done to reflect the pH of MilliQ water, which is usually around 5.6 at ambient conditions.[36,37] It is believed that these slightly different conditions still reasonably reflect the conditions of the neutral isotope harvesting water. For our experiments, this was aimed to be around pH 5.6, which was achieved without the use of any buffers to keep the level of background ions at a very low level. After each stock solution was prepared according to the description in section 2.2.2, four solutions were made that comprised the individual elements, diluted to about 1ppm with MilliQ water. Individually, solution 1 encompassed cobalt, copper, and manganese, solution 2 consisted of arsenic, selenium, and zinc, solution 3 of nickel and scandium, and solution 4 of chromium and vanadium. The pH of each solution was adjusted to 5.6±0.1 using dilute solutions of sodium hydroxide (NaOH) and HNO_3, together with a multi-point calibration pH meter (Seven Compact™ Duo S213 pH/Conductivity Meter). After this initial adjustment, each solution was left to equilibrate overnight, after which the pH was checked and re-adjusted, if necessary.

After the equilibration and final pH adjustment, the prepared metal solutions were used for the adsorption experiments with the metal oxides. A mass of about 100mg of each metal oxide was weighed out in triplicate for each tested solution into 25mL Eppendorf tubes. To each tube, 10mL of each test solution was added. A blank solution with no added metal oxide powder was also included with each test series. The samples were placed inside a shaking incubator (New Brunswick Innova 42 Incubator) set to 300rpm at 20°C for 24 hours. After the incubation period, the samples were centrifuged three times in a Sorvall ST8 benchtop centrifuge (ThermoFisher Scientific) at 4000rpm for 10 minutes. After centrifugation, two layers formed: the metal oxide which contained any of the potentially adsorbed elements, and the supernatant which contained the un-adsorbed elements. The supernatant solutions were carefully transferred into separate 25mL tubes.

2.5: ICP-OES Analysis

For ICP-OES analysis, all samples, which included all supernatants, sample blanks, and aliquots of the initial test solutions, were diluted in a 1:2 and 1:3 ratio with 3% HNO_3 as the matrix. A series of five standards at concentrations of 0.01, 0.05, 0.1, 0.5, and 1ppm respectively, which included all elements that were present in the samples, were prepared with 3% HNO_3 as the

matrix. The 3% HNO_3 solution also served as the measurement blank.

2.6: Point of Zero Charge (PZC) Determination

To determine the PZC for each metal oxide, 12 solutions were prepared: six solutions of MilliQ water and six solutions of 0.1M sodium nitrate ($NaNO_3$). Using the pH meter, the pH of each solution was adjusted using dilute solutions of either HNO_3 or NaOH to create a series with pH 2, 4, 5, 6, 8, and 10. After adjustment, 20mL of each solution was added to pre-weighed 25mL tubes that contained about 100mg of metal oxide. The samples then were placed inside the incubator shaker, set to 300rpm at 20°C for 24 hours. Post-incubation, the samples were centrifuged at 4000rpm for 10 minutes, and the supernatant of each solution was transferred into a new 25mL tube. The pH of each supernatant was determined and used to calculate the ΔpH. Using the initial pH of each solution and the ΔpH, the PZC plot of each metal oxide was generated.

2.7: X-Ray Diffraction (XRD)

Powder XRD is a frequently used technique for the characterization of materials, providing information on the sample composition and phase identification.[38] The characterization of each metal oxide allows for a comparison of the vendor-provided speciation with experimental data. Figure 4 includes all resulting spectra for each metal oxide, excluding silicon dioxide, against a reference spectra from the COD. A summary of the tested metal oxides and the best phase matches are given in Table 3. The results match with what is expected from the vendor information, with no significant impurities or other elements that could compromise any subsequent experiments. Of all the tested compounds, silicon dioxide was unable to generate an XRD spectrum. The utilized silicon dioxide is amorphous, which results in output signals of low intensities.[39]

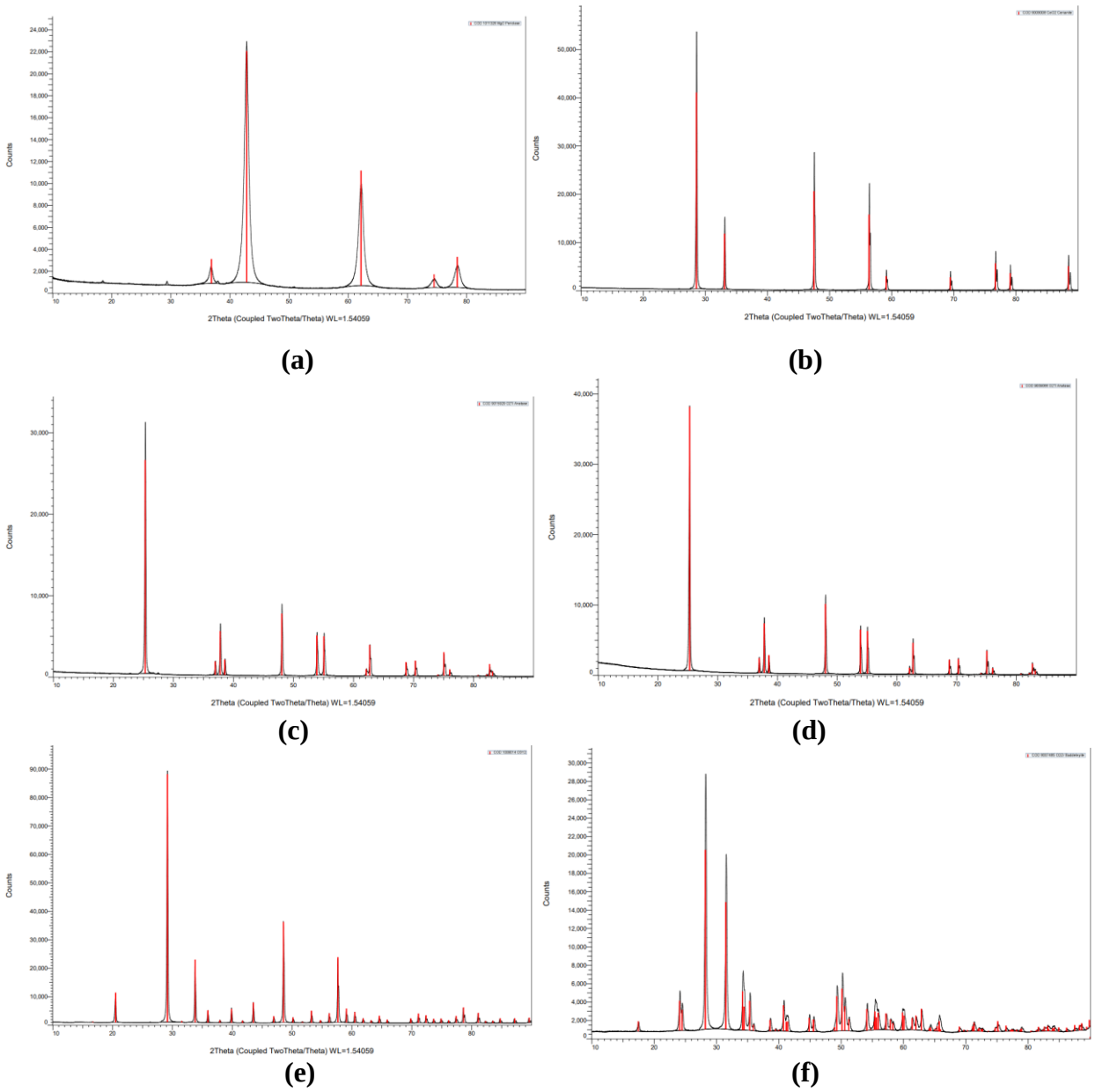

Figure 4: Powder XRD spectrum, with reference spectrum (red lines), of (a) Magnesium oxide. (b) Cerium (IV) oxide. (c) Titanium dioxide. (d) Titania nanoparticles. (e) Yttrium (III) oxide. (f) Zirconium (IV) oxide.

Table 3: List of all tested metal oxides, the reported phases are the ones with the best match from the database.

ID	Phase	1st Match %
ZrO_2	monoclinic	70
Y_2O_3	cubic	98
CeO_2	cubic	76
MgO	cubic	96
TiO_2	tetragonal	99
TiO_2 (NP)	tetragonal	99
SiO_2	amorphous	----------

2.8: Point of Zero Charge Data

When making PZC plots of each metal oxide, sodium nitrate was included as a matrix alongside MilliQ water. It is predicted that electrostatic interactions govern the adsorption of the elements onto the oxides; however, electrolyte-specific effects could influence element adsorption. As a result, most literature that determine the PZC of metal oxides do so with a background electrolyte.[40,41] The tests were done with sodium nitrate solution to be comparable to the literature PZC, as well as in MilliQ water to simulate the conditions during the isotope harvesting process.

By determining the PZC of each metal oxide, the pH at which the surface charge is zero will be elucidated. The surface charge is an important parameter in the adsorption of metals onto metal oxide surfaces. Figure 5 lists all the generated PZC plots for each metal oxide. Looking at the PZC plot for zirconium (IV) oxide, the PZC is at around pH 4; given the pH of the water solution is 5.6, zirconium (IV) oxide is expected to have a negatively charged surface. Yttrium (III) oxide has its PZC at roughly pH 7, therefore yttrium (III) oxide should have a positively charged surface. From the PZC plots, it also is evident that the PZC exhibited no major differences between the MilliQ water and sodium nitrate matrices. Table 4 is a summary of all the metal oxide PZC pH, and the expected surface charge at the pH of the isotope harvesting water, alongside some literature PZC. It is worth noting that the literature data on the PZC with metal oxides varies strongly, depending on the tested matrix (background electrolytes), methods done (instrument, pre-conditioning, etc.), and manufacturer information (morphology, particle size,

etc.). While most of the here acquired data agree with the provided literature PZC, those that deviate, such as zirconium (IV) oxide and titanium dioxide, can be attributed to the inclusion of the background electrolytes and differences in the metal oxide material.[41]

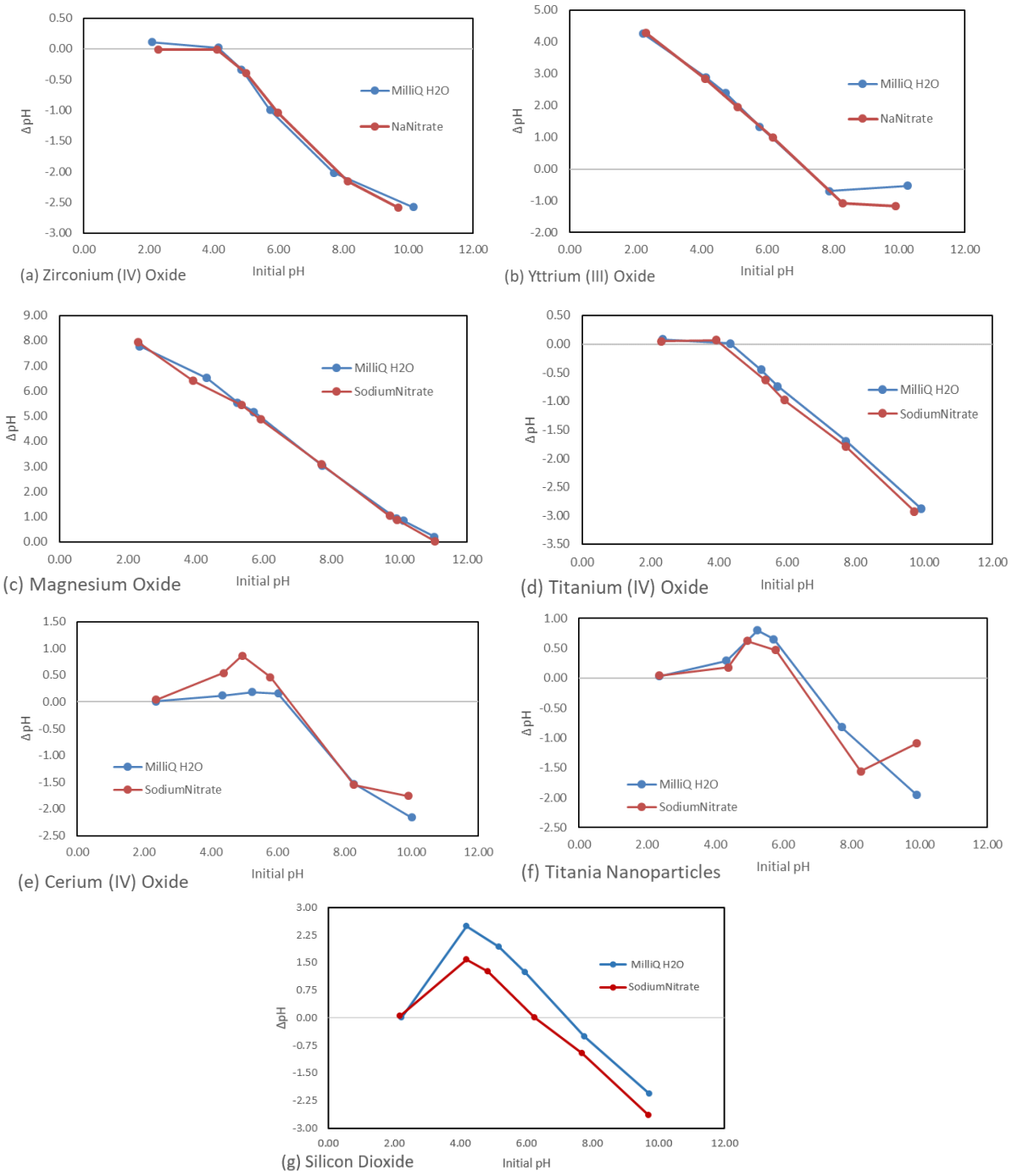

Figure 5: PZC plot of (a) Zirconium (IV) oxide*. (b) Yttrium (III) oxide*. (c) Magnesium oxide*. (d) Titanium (IV) oxide*. (e) Cerium (IV) oxide*. (f) Titania nanoparticles*. (g) Silicon dioxide. (*data was collected by Suvan Campbell)

Table 4: List of all the tested metal oxides, the pH PZC, the expected surface charge at pH 5.6, and a set of literature PZC data for comparison.[41] (*data was collected by Suvan Campbell)

Metal Oxide	PZC	Literature PZC	Expected Charge (at pH 5.6)
Zirconium (IV) Oxide	~4	6.1	**(-)**
Yttrium (III) Oxide	~7	7.5	**(+)**
Magnesium Oxide	~11	9.8	**(+)**
Titanium (IV) Oxide*	~4	6	**(-)**
Cerium (IV) Oxide*	~6.5	6	**(+)**
Titania Nanoparticles*	~7	6	**(+)**
Silicon Dioxide	~7	<5	**(+)**

2.9: Pourbaix Diagrams

In tandem with the PZC of the metal oxide, another parameter to consider is the charge of each species in solution. The pH of the surrounding solution impacts the charge of the metal oxide surface; additionally, the pH can also influence the expected charge of each element in the water. Pourbaix Diagrams visualize the expected speciation of an element by plotting its electrochemical potential (E_h) against the pH in an aqueous solution.[42] The diagrams referenced in this experiment can be found in a compilation of Pourbaix Diagrams.[43] Figure 6(a) shows the Pourbaix Diagram of zinc. Due to the aerated environment of the adsorption experiment, it is expected that the solutions rather have a positive potential. This is also expected for the water during isotope harvesting, where the generated hydrogen peroxide due to radiolysis creates a strongly oxidative environment.[18] For a pH of 5.6, zinc is predicted to exist as a Zn^{2+} cation over a broad range of electrochemical potentials.[44] Table 5 lists the expected charge of each species in the performed experiment.

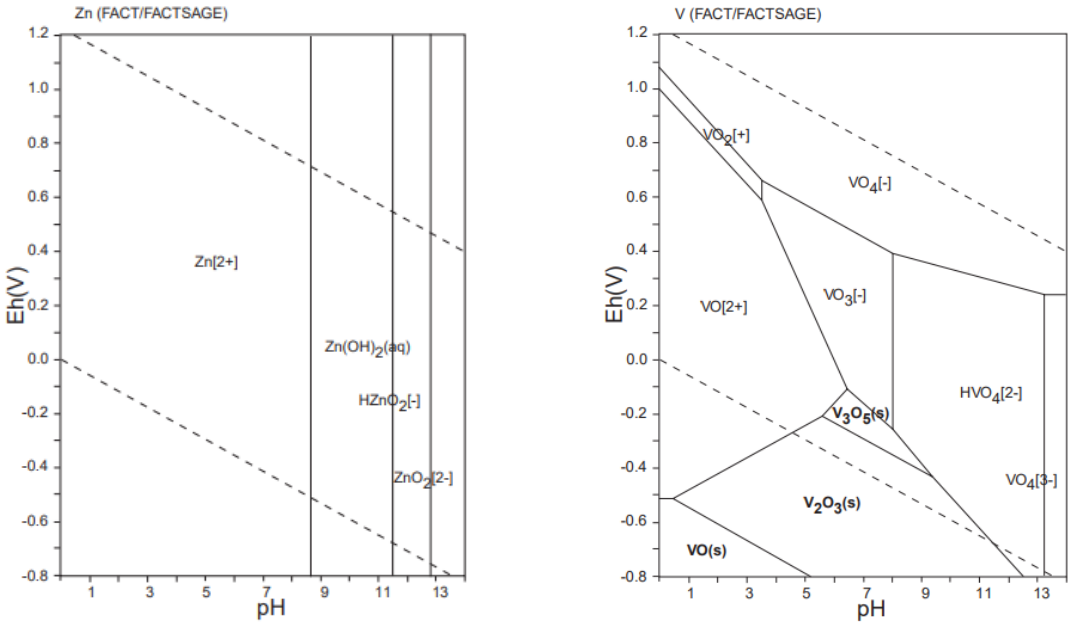

(a) **(b)**

Figure 6: (a) Pourbaix Diagram of Zinc. (b) Pourbaix Diagram of Vanadium.[43]

Table 5: List of the expected species and charge of each element at pH 5.6 from their respective Pourbaix Diagrams.[43]

Element	Expected Charge (at pH 5.6)
Arsenic	(-)
Chromium	(-)
Cobalt	(+)
Copper	(+)
Manganese	(+)
Nickel	(+)
Scandium	(+)
Selenium	(-)
Vanadium	(-)
Zinc	(+)

However, these predictive estimations are subject to certain limitations, since the precise electrochemical potential of the water is not well known and is also subject to changes. Looking for example at Figure 6(b) and the Pourbaix Diagram of vanadium, a higher potential could see the dominant species from solid vanadium to VO_3[-] and would then have a negative charge. In

addition, multiple species of each element may also still be present in solution.

2.10: Adsorption Data

Using ICP-OES, the adsorption of each element onto the metal oxides was quantified. Figure 7 and 8 are the adsorption data for each metal oxide. The PZC and Pourbaix Diagrams do explain some of the adsorption mechanisms for the metal oxides. For example, chromium showed strong adsorption onto yttrium (III) oxide (99.8%). The PZC data supports that yttrium (III) oxide has a positively charged surface, and the Pourbaix Diagram of chromium suggests that it is present as an anion in solution, so electrostatic attractions allow for efficient adsorption. There are exceptions to these interactions since many of the metal oxides still demonstrated strong adsorption to a wide variety of elements. Silicon dioxide showed strong adsorption for zinc (98.9%), but the PZC suggests a positively charged surface, while the Pourbaix Diagram also predicts a cationic species, leading to the expectation of electrostatic repulsions that translate to a low adsorption. Aside from Van Der Waals interactions, there can also be chemisorption of the elements onto the metal oxide surfaces; the presence of hydroxy species could allow for the precipitation of specific elements that otherwise would not adsorb due to charge. There also can be other chemical interactions occurring in solution, like the formation of metal aquo complexes, which can affect the adsorption of particular elements. Other effects on adsorption can include the radius of the adsorbed species, as well as the particle size of the metal oxides.[45–48] Magnesium oxide demonstrated the best adsorption across all 10 elements and the PZC data (pH ~11) supports a basic nature. There would be a surplus of hydroxy ions present in solution, leading to the formation of hydroxy species with subsequent precipitation onto the magnesium oxide surface.

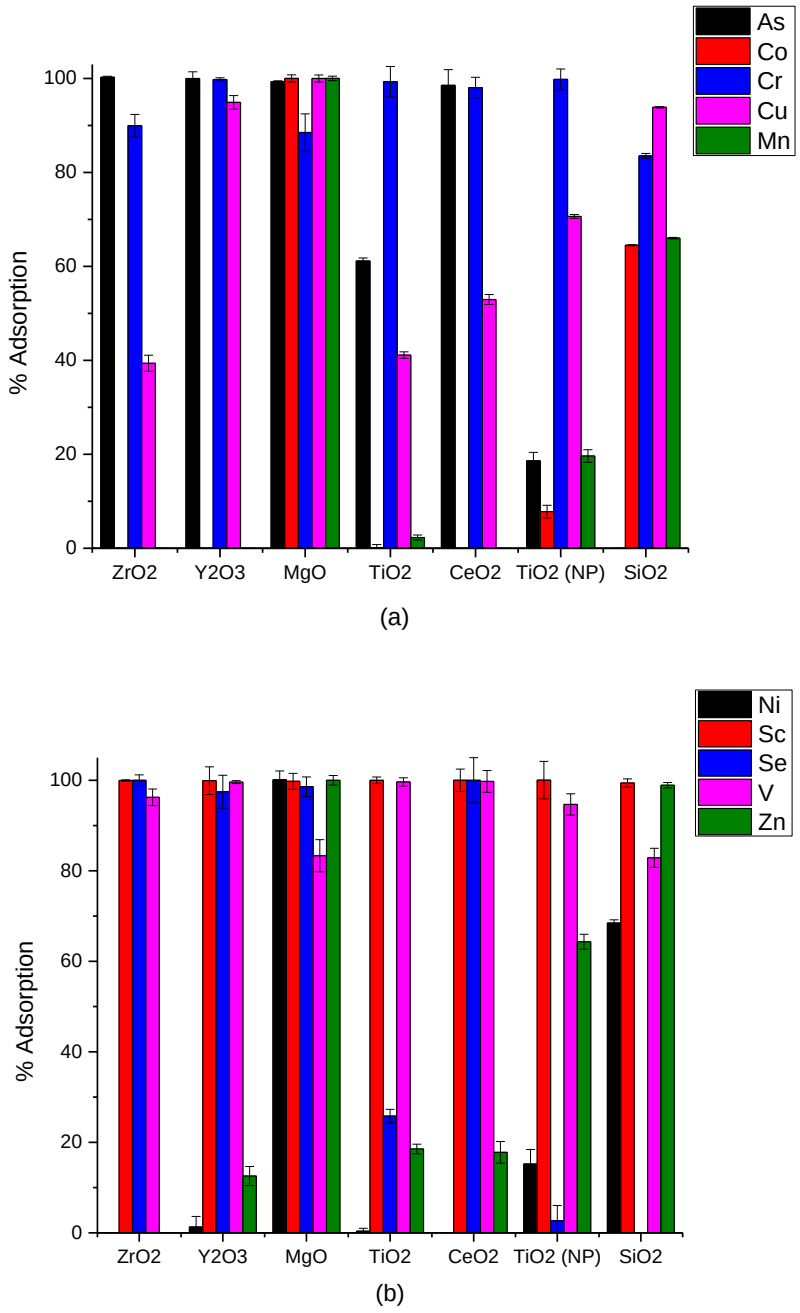

Figure 7: (a) Adsorption plot of the seven tested metal oxides for arsenic, cobalt, chromium, copper, and manganese. (b) Adsorption plot of the seven tested metal oxides for nickel, scandium, selenium, vanadium, and zinc.

	MeOx Charge	As	Co	Cr	Cu	Mn	Ni	Sc	Se	V	Zn
Expected Species Charge	X	(-)	(+)	(-)	(+)	(+)	(+)	(+)	(-)	(-)	(+)
Zirconium (IV) Oxide	(-)	100.0	~0	89.9	39.4	~0	~0	100.0	100.0	96.2	~0
Yttrium (III) Oxide	(+)	100.0	~0	99.8	94.9	~0	1.3	99.9	97.5	99.6	12.6
Magnesium Oxide	(+)	99.4	100.0	88.5	100.0	100.0	100.0	99.8	98.6	83.3	100.0
Titanium (IV) Oxide*	(-)	61.1	0.1	99.3	41.1	2.3	0.4	100.0	25.8	99.6	18.5
Cerium (IV) Oxide*	(+)	98.5	~0	98.1	52.9	~0	~0	100.0	100.0	99.8	17.8
Titania Nanoparticles (100nm) 10 mg*	(+)	18.6	7.8	99.8	70.6	19.6	15.2	100.0	2.7	94.7	64.3
Silicon Dioxide	(+)	~0	64.5	83.5	93.9	66.0	68.5	99.4	~0	82.9	98.9

Figure 8: Data of the percent adsorption of the 10 elements to each of the tested metal oxides, alongside the expected species charge and metal oxide charge at pH 5.6. (*data was collected by Suvan Campbell).

The obtained data suggests that selected metal oxides are more efficient in adsorbing certain species than others, which could be applicable for selectively adsorbing particular species. Magnesium oxide, however, demonstrated the best adsorption across all 10 elements, showing promise as a broad-range sorbent material. A concern with the use of magnesium oxide is its partial water solubility, which could limit its application as a sorbent material for isotope harvesting.

2.11: Equilibration of Silicon Dioxide

It was evident that magnesium oxide demonstrated suitable sorbent capabilities, which were limited by the partial solubility in water. The concern was if any of the metal oxides were used as a sorbent for the water dump system, they would introduce ions to the water. A potential solution was to examine if equilibrating the metal oxide surface would mitigate the ability to alter the solution pH. It was determined whether the pre-equilibration of silicon dioxide in water, as it is water-insoluble, would demonstrate a comparable PZC and similar adsorption to the non-

equilibrated SiO_2. An aliquot of the stock silicon dioxide powder was vortexed with 20mL of MilliQ water and left to equilibrate. The silicon dioxide was vacuum-filtrated and dried at elevated temperatures to remove any excess water. The PZC of the equilibrated silicon dioxide was determined as outlined in section 2.2.5. Figure 9 highlights the PZC plots for both normal silicon dioxide and the equilibrated silicon dioxide. The data highlights minimal differences in PZC (~6.5) with the normal and equilibrated oxides, demonstrating that equilibrating the metal oxides would not mitigate its ability to alter the solution pH.

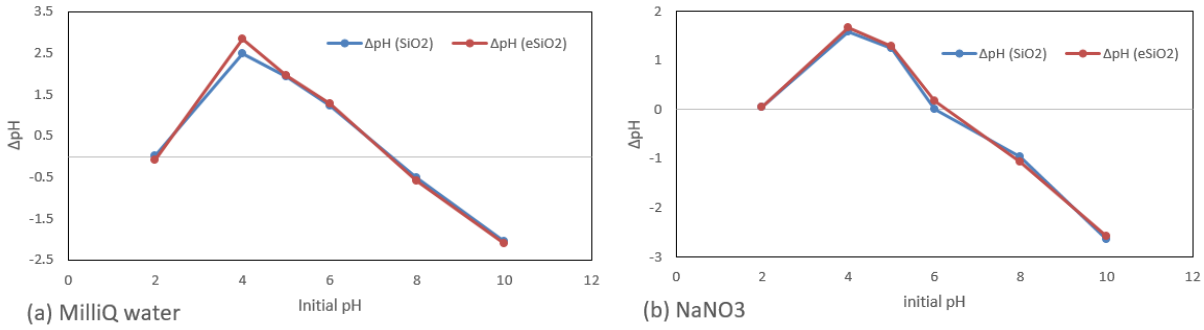

Figure 9: (a) PZC plots of the equilibrated silicon dioxide versus the non-equilibrated silicon dioxide in MilliQ water. (b) PZC plots of the equilibrated silicon dioxide versus the non-equilibrated silicon dioxide in sodium nitrate.

Another potential solution would be to implement other sorbent materials. Graphite was considered as an inexpensive sorbent for isotope harvesting. The examination of the adsorption capability followed the same procedures outlined from section 2.2.2 to section 2.2.4. However, the poor adsorption capability of graphite across the 10 elements (shown in Table 6) precluded any further investigations.

Table 6: Adsorption data of graphite for the 10 tested elements.

Element	% Adsorption
Mn	0
Co	1.23 ± 0.22
Cu	16.12 ± 0.67
Se	1.85 ± 0.43
As	12.54 ± 2.59
Zn	0
Ni	0

Table 6 (cont'd)

Sc	11.83 ± 1.12
Cr	15.70 ± 0.75
V	17.93 ± 3.95

2.12: Stable ^{61}Ni Experimentation

The promising adsorption capability of magnesium oxide towards most tested elements, particularly towards nickel, promoted the preparation of a sample to test the applicability for mass separation and the high-temperature environment of the BMIS. For this, a stock solution of stable ^{61}Ni (99.42% isotopic enrichment, Isoflex USA) was prepared, following the procedure outlined in section 2.2.2. The adsorption procedure onto magnesium oxide followed similar steps outlined in sections 2.2.3 to 2.2.4, with nickel-61 chloride as the only solution. After separating the supernatant, the magnesium oxide was left inside a fume hood to evaporate any residues of water. For the mass-separation experiment, a sample mass of about 1µg ^{61}Ni ($9.88*10^{15}$ atoms) was utilized, which translated to 21mg dried magnesium oxide that was transferred onto a 50x50mm sheet of 0.006mm thickness tantalum foil (99.9% purity, GoodFellow).

The stable sample was folded up and inserted into the BMIS for ^{61}Ni extraction. Nitrogen trifluoride (NF_3) gas was used during evaporation to help volatilize the sample. Several mass scans were recorded at different temperature conditions. Figure 10 shows all mass scans taken from this experiment. It is evident from the mass scans that ^{61}Ni formed many complex species with the magnesium oxide and the introduced fluorides from NF_3. With the oxygen, many refractory oxygen-containing compounds formed, which rendered the extraction from BMIS highly challenging and resulted in low yields. Additionally, the amount of ^{61}Ni was distributed over many different species, thereby reducing the current available for extraction of one single mass. Considering the challenges in preparing the adsorbed metal oxide samples and extracting a viable current from the BMIS, it was concluded that metal oxides are not particularly suitable as target materials for metallic radionuclides. Therefore, it was decided to disconnect the collection of isotopes and the preparation of samples for mass separation. This provides the option to include a chemical pre-separation step to produce cleaner samples and also offers more flexibility to tailor the targetry for the mass-separation step.

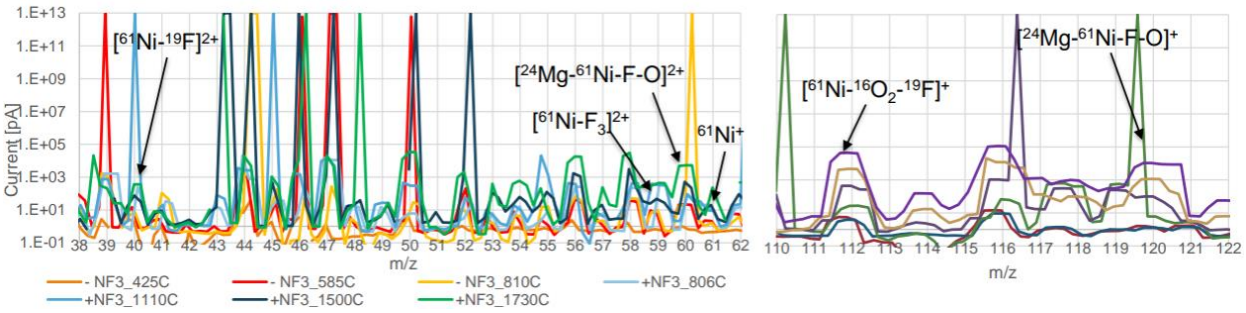

Figure 10: Mass scans of the stable ^{61}Ni on magnesium oxide across several temperatures inside BMIS, with and without the addition of NF_3.

2.13: Conclusions and Future Directions

The adsorption of 10 stable elements was simulated onto metal oxides to determine future applications towards isotope harvesting. The use of metal oxides could allow for a seamless combination of harvesting isotopes and mass separation. After analyzing several metal oxides, magnesium oxide was determined to be the most efficient in adsorbing all interesting species. However, it was evident that certain metal oxides, particularly magnesium oxide, would drastically shift the aqueous solution pH, introducing ions into solutions that should be avoided if applied to the water-dump system. Equilibrating the metal oxide surface was done using silicon dioxide as a potential solution, though it was not able to mitigate these pH changes. A first mass-separation experiment involving a sample of stable ^{61}Ni adsorbed onto magnesium oxide was performed. However, the extraction of ^{61}Ni from the oxide matrix proved exceedingly difficult, compounded by less than satisfactory adsorption chemistry. Subsequently, it was concluded to disconnect the isotope harvesting and mass-separation steps, as this offers additional advantages of implementing a chemical pre-separation and to have more flexibility for tailoring the targetry. While the results indicated limited applicability of metal oxides as target materials for the BMIS, the adsorption of specific elements on certain metal oxides could be useful for specific applications. For example, while magnesium oxide is not suitable for aqueous harvesting due to its partial water solubility, silicon dioxide is an insoluble oxide that has a negligible effect on the water pH and could be useful for specific harvesting tasks. Species such as copper and zinc showed good adsorption onto SiO_2, indicating a potential application for collection.

CHAPTER 3: Preparation of Source Samples for the BMIS

3.1: ^{73}As Source Sample Preparation

The following work is intended for submission as a Short Communications paper to the Journal of Applied Radiation and Isotopes, entitled as "Preparation of a ^{73}As Source Sample for Application in an Offline Ion Source." For the purpose of this thesis, the text presented here has been rephrased.

3.2: Background

The Facility for Rare Isotope Beams (FRIB) is a state-of-the-art national research facility dedicated to advancing nuclear science. Typically, rare isotope beams crucial for cutting-edge research are generated through the fragmentation of stable primary beams.[49] However, for specific user experiments, ion beams can be alternatively produced in what is termed 'offline mode' using either radioactive or stable source samples.[28] One such radioisotope, ^{73}As, notable for its 80.3-day half-life and primary gamma-ray emission at 53.437keV (I_γ=10.6%), finds application in nuclear data studies and cross-section measurements in nuclear astrophysics.[50–52] A possible way to produce ^{73}As beams for user experimentation at FRIB is through using source samples inside the Batch Mode Ion Source (BMIS). BMIS is an oven-ion source combination, where the introduced source samples undergo evaporation and atomization within the oven, followed by ionization in the plasma ion source. A mass analyzer selects the desired ion beams before transmission through the beamline for diverse research endeavors.[28] These beams can be directed to the Re-Accelerator (ReA) or to other various user end stations, including the Low-Energy Beam and Ion Trap facility (LEBIT), the Beam Cooler and Laser Spectroscopy facility (BECOLA), and a beamline for experimenter instrumentation.[53,54] Notably, the offline configuration of BMIS enables independent operation of these stopped and reaccelerated beam facilities, allowing concurrent execution of multiple user experiments at FRIB.[27,28] Since coming online in 2021, the BMIS team has successfully delivered a chosen set of offline-generated isotope beams for user experiments.

A suitable source sample for BMIS must meet several criteria. The material must be solid and readily vaporizable within BMIS operating temperatures (ranging from approximately 300ºC up to generally ~1000 ºC, but temperatures up to 2000ºC are possible). Additionally, volatile matrix components and isobaric impurities shall be minimized or eliminated. Responding to the strong interest from the FRIB user community for a low-energy ^{73}As beam, this paper outlines the preparation of a ^{73}As source sample to support the experimental user beam program at FRIB.

Utilizing an acidic ^{73}As solution, silver arsenate was produced due to its favorable volatility within the BMIS operating temperature range. This conversion was achieved through an optimized precipitation reaction after the addition of a stable arsenic carrier. Ultimately, a source sample containing approximately 1.6mCi ($5.76*10^{14}$ atoms) of ^{73}As was prepared and effectively utilized in BMIS to provide a ^{73}As beam for user experimentation.

3.3: Stable and Radioactive Arsenic Isotopes for Sample Preparation

The ^{73}As solution was sourced from the National Isotope Distribution Center (NIDC), with an initial activity of 3mCi. It contained less than 0.01mCi of ^{74}As and was in a 0.1N hydrochloric acid (HCl) matrix. Stable arsenic was obtained from a +3 arsenic ICP solution from High-Purity Standards (HPS), with a concentration of 1000 ± 20ppm As in a 2% HCl matrix.

3.4: Chemicals

To prepare the source samples, hydrogen peroxide (H_2O_2, 30%, ACS grade, Fisher Scientific), glacial acetic acid (CH_3COOH, ≥99%, GR-ACS, Millipore Sigma), ammonium hydroxide solution (NH_4OH, 30%, Sigma Aldrich), hexane (C_6H_{14}, Supelco, Sigma Aldrich), and silver nitrate ($AgNO_3$, Reagent ACS, ChemPure Brand Chemicals) were utilized. Stable element analysis was conducted in a 3% volume matrix of nitric acid (HNO_3, 70%, Sigma Aldrich). A 50x50mm sheet of tantalum foil with a thickness of 0.006mm (99.9% purity, GoodFellow) served as the support material, while acetone (C_3H_6O, for liquid chromatography, Supelco, Sigma Aldrich) was used for rinsing. MilliQ water with a conductivity of 18.20MΩ*cm obtained from a Thermo Scientific Barnstead MicroPure Water System was used for all dilutions. Stock solutions of ICP arsenic standard (997mg/L ± 4mg/L, 5% HNO_3 matrix, Sigma Aldrich) and ICP silver standard (Transition Metal Mix 1 for ICP, 100mg/L, 2% HNO_3 matrix, Sigma Aldrich) were employed for the stable element analysis.

3.5: Instruments

Inductively Coupled Plasma-Optical Emission Spectroscopy (ICP-OES, Agilent 5900) was employed for the analytical determination of stable element concentrations. The activity of ^{73}As was quantified using a High-Purity Germanium Detector (HPGe, BEGe gamma-ray detector, BE2020, Canberra), using the characteristic gamma-line at 53.43keV, with I_γ=10.6%. Energy and efficiency calibration were conducted using europium-154 (Eu-154, Eckert & Ziegler, 1.054μCi, reference date 15-Sep-2020, E_γ=123.07keV (40.4%), 247.92keV (6.89%), 591.75keV (4.95%), 723.30keV (20.06%), 873.18keV (12.08%), 1004.76keV (18.01%), 1274.42keV (34.8%)) and

americium-241 (Am-241, Eckert & Ziegler, 1.040μCi, reference date 15-Sep-2020, E_γ=59.54keV (35.9%)) point sources, positioned at distances of 15cm, 25cm, and 100cm.

For characterization purposes, Scanning Electron Microscopy-Energy Dispersive X-Ray (SEM-EDS, JEOL 7500F, Oxford Instruments AZtec system) analysis and X-Ray Photoelectron Spectroscopy (XPS, CasaXPS, Physical Electronics 5400 System) were employed on the prepared stable arsenic source samples. Chemical processing utilized a benchtop vortex mixer (Digital Vortex Mixer, VWR), a hot plate (Cimarec, Barnstead Thermolyne), and a benchtop centrifuge (Sorvall ST8, ThermoFisher Scientific).

3.6: Stable Silver Arsenate Precipitation

The stable arsenic used was sourced from a +3 arsenic ICP solution that had to be converted to the +5 oxidation state by adding 1mL of the 1000ppm As3+ solution to 30% hydrogen peroxide at a 1:5 volumetric ratio.[55] This solution was covered and left at room temperature overnight; subsequently, the solution was evaporated completely at 90ºC. The resulting residue in the sample container was dissolved in approximately 500μL MilliQ water and transferred to an Eppendorf tube. The beaker was rinsed three times with MilliQ water, and the rinse solutions were also added to the tube.

The precipitation process followed a similar procedure outlined by L. J. Curtman and P. Daschavsky.[56] A stock solution of silver nitrate was prepared at a concentration of 5000ppm Ag and stored in the dark to prevent photo-reduction. Around 0.5mL of the prepared As(V) solution, containing 80μg As, was used for precipitation. Silver nitrate stock solution was added to achieve molar ratios of Ag:As of 1.3:1, 5.7:1, and 12.7:1. The pH of the solution was adjusted to 7-8 using a few drops of 1M ammonium hydroxide and 10% acetic acid. After pH adjustment and vortexing, a visible brown precipitate formed. The sample was sealed with parafilm and left to react overnight. The mixture was then centrifuged, and the supernatant was separated off and transferred to another tube. The concentrations of arsenic and silver in the supernatant were quantified via ICP-OES to assess the precipitation yield.

3.7: Stable Source Sample Preparation

The stable silver arsenate precipitate, prepared with an optimized Ag:As ratio of 5.7:1, was utilized for the preparation of stable source samples. A 50x50mm sheet of tantalum foil was used as the support material; this sheet was cleaned with acetone and left to air-dry. The precipitate was suspended in solution and transferred onto the foil, which was kept inside a small,

in-house-made aluminum boat. The entire assembly of the foil and aluminum boat was placed on a hot plate set to 150ºC to evaporate off the solution. Any remaining silver arsenate was rinsed from the tube three times with approximately 0.6mL hexane, pipetted onto the foil, and evaporated. These stable samples were employed to develop the beam extraction from the BMIS and optimize the ion beam delivery process. Additionally, the prepared stable source samples were characterized by SEM-EDS and XPS to identify the present elements, their relative atomic percentages, and obtain further information about compound speciation.

3.8: ^{73}As Precipitation and Source Sample Preparation

Activity monitoring was maintained throughout the precipitation process to track radiation levels and adjust for any activity losses. A volume of 0.259mL of the ^{73}As solution, containing 2.8mCi of ^{73}As, was utilized for the reaction. To facilitate quantitative precipitation of the radioactive arsenic, the ^{73}As sample was spiked with 80µg of stable arsenic (equivalent to 27.2µL of a 2949ppm stable As solution). The oxidation with 30% H_2O_2 and the subsequent steps for stable precipitate formation (section 3.2.4) were done by following the optimized procedure for stable precipitate formation. After oxidation and evaporation, the reconstituted solution (287.2µL) was employed for the precipitation reaction. This involved using the previously optimized 5.7:1 ratio of Ag:As and adjusting the pH of the solution to 7-8. Once visible precipitation occurred and incubation was completed, the precipitate was separated via centrifugation and the supernatant was removed. The resulting precipitate was utilized for source sample preparation. The radio-silver arsenate was transferred onto a clean sheet of tantalum foil on a hot plate set to 150ºC. During transfer and subsequent rinsing of the tube using hexane, the sample activity was monitored, ensuring approximately $6.67*10^{14}$ atoms (1.8mCi) of ^{73}As were transferred onto the tantalum foil. The prepared source sample was transported to FRIB and utilized for generating the ^{73}As beam.

3.9: ^{73}As Beam Delivery

The tantalum foil covered with ^{73}As was tightly folded and inserted into the BMIS oven. The oven was heated to 500-1000ºC, causing the sample material to evaporate, followed by effusion into the ion source. Through ionization, monovalent $^{73}As^+$ ions were formed, and the resulting ion beam was extracted, containing $^{73}As^+$, stable ^{75}As, and other contaminants. Following acceleration to 30keV, the beam underwent mass separation, with the desired $^{73}As^+$ ions being selected and further accelerated to low energies in the ReAccelerator, allowing for

successful delivery to the scientific low-energy beam program.

3.10: Stable Silver Arsenate Source Sample Preparation

Arsenic +3 compounds are typically highly volatile, which may lead to considerable losses during subsequent sample preparation procedures.[57] Initial explorations into evaporating a stable arsenic (III) solution showed recoveries below 0.5%. However, upon the addition of hydrogen peroxide at a five-fold molar excess, the arsenic in solution was oxidized to the less volatile +5 oxidation state. This transformation was validated by achieving arsenic recovery rates of approximately 100% after evaporation.

In order to ensure complete precipitation of a low-mass arsenic sample of 80μg, multiple experiments were conducted to determine the optimal Ag:As ratio. The selected low amount of stable As represents the upper limit of stable arsenic carrier, which is in alignment with the chemical toxicity limit set by the Occupational Safety and Health Administration (OSHA) for the specific space settings in the accelerator vault. This amount was consistently applied throughout the optimization process. With a 1.3-fold ratio of Ag, the quantitative formation of silver arsenate was induced, resulting in a precipitation yield of around 95% (±4.12%) (see Figure 11). However, complete precipitation of 100% (±4.24%) was achieved with 5.7- and 12.7-fold excesses of Ag. Based on these findings, the 5.7:1 ratio of Ag:As was chosen to ensure optimized precipitation yields of silver arsenate while minimizing the silver amount in the sample. Notably, the ICP-OES analysis of the silver in the supernatant suggested a silver depletion that would support the presence of an approximate 3:1 stoichiometric ratio of Ag:As in the precipitate.

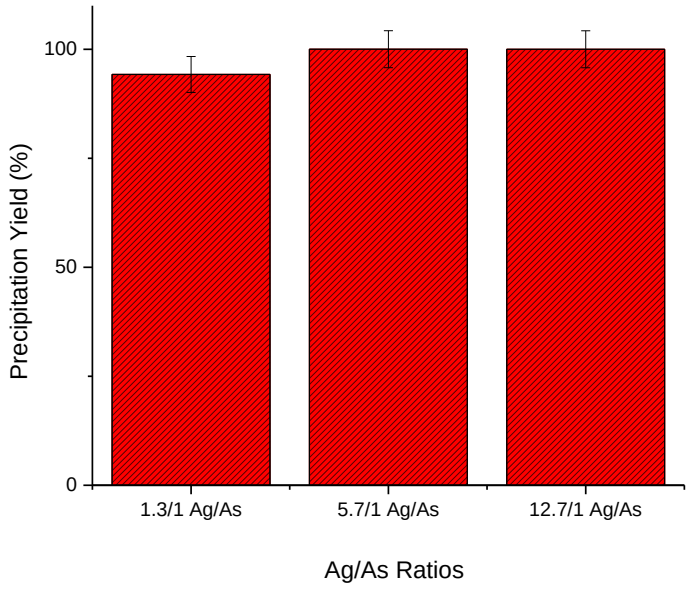

Figure 11: Bar graph of the percent stable arsenic precipitated with different ratios of silver. Quantification was done via ICP-OES. The error bars include the propagated error from the ICP-OES analysis and the respective dilution factors.

3.11: ^{73}As Source Sample Preparation

Once the optimized method was established through stable arsenic experiments, it was applied to create a silver arsenate precipitate with the radioactive ^{73}As material. Despite the typically high volatility of arsenic compounds, utilizing them for source samples in BMIS would lead to rapid depletion and limited ion rates towards the end of extended beam experiments. Given that the melting point of silver arsenate is 830ºC, falling within the operational temperature range of BMIS, it was deemed suitable for sustaining adequate beam rates over prolonged durations.[58]

Throughout the formation of the radio-silver arsenate precipitate and the preparation of the source sample, activity levels were consistently monitored via gamma-spectroscopic measurements. The formation of silver arsenate was highly quantitative, with only 0.013mCi of ^{73}As (±0.00040mCi) remaining in the supernatant. This indicates a precipitation yield of 99.4%, which is comparable to the stable arsenic sample preparation achieving a 100% yield. However, during the transfer of the precipitate onto the tantalum foil, 0.698mCi of ^{73}As (±0.0179mCi) adhered to the pipette tip and the surface of the Eppendorf tube. Despite multiple rinse cycles with hexane, only µCi quantities of ^{73}As could be removed. Following the transfer of 1.556mCi of ^{73}As

(±0.1011mCi) onto the tantalum foil, the resulting source sample was introduced into the BMIS oven. A significant loss of 0.512mCi (±0.0168mCi) of ^{73}As occurred due to adsorption onto the surface of the Eppendorf tube, while the rest was lost to the pipette tips. However, in retrospect, rinsing with 2mL of 3% HNO_3 was identified as an effective method for removing any residual ^{73}As, leaving only 0.0183mCi of ^{73}As in the tube after this step. These findings could be of importance for future source sample preparation endeavors.

3.12: Sample Characterization via SEM-EDS

Due to certain analytical instruments not being approved for handling radioactive materials, characterization was conducted using stable source samples, as their chemical behavior was anticipated to mirror that of the radioactive samples. Following the outlined procedure, it was anticipated that the arsenic sample would generate silver arsenate with arsenic in the +5 oxidation state. Scanning Electron Microscopy coupled with Energy-Dispersive X-ray Spectroscopy (SEM-EDS) provided insights into the morphology of the stable arsenic precipitate and identified the constituent elements. Figure 12(a) depicts a section from a large part of the precipitate on the foil. The prepared source sample exhibited an irregular morphology, featuring regions entirely covered with precipitate interspersed with sections of exposed tantalum substrate (the darker regions in Figure 12(a)). Variations in drying rates could lead to an uneven distribution of the precipitate on the foil. Nevertheless, this uneven distribution did not hinder the application of the samples in the ion source. Figure 12(b) illustrates one EDS spectrum taken from point 1 on the map (indicated as Spectrum 1 in Table 7). The presence of predominant species, including silver, arsenic, and oxygen, was expected from each spectrum. To characterize the precipitate, spectra were taken from three different regions of the precipitate. The obtained data from recording these spectra (Spectra 1-3) are presented in Table 7. Spectra 1 and 2 were taken from spots in the central region, while Spectrum 3 was recorded on an edge region of the section in Figure 12(a). The EDS analysis indicated the presence of carbon, likely derived from the hexane rinses employed during the transfer of the precipitate onto the tantalum substrate. The atomic percentages of silver, arsenic, and oxygen were utilized to estimate the stoichiometric ratios of each element within the precipitate. The stoichiometric ratios between Ag, As, and O in Spectra 1 and 2 would allow to assume the presence of either silver arsenate (Ag_3AsO_4) or silver arsenite (Ag_3AsO_3). Both compounds exhibit an Ag-to-As ratio of 3 to 1, a finding corroborated by the ICP-OES analysis, which also indicated this 3:1 ratio. However, obtaining reliable quantitative estimates for oxygen

through EDS is challenging. Therefore, the oxygen amount was not used to determine the specific silver-arsenic compound. Spectrum 3 however, suggests a considerably higher Ag:As ratio. This spectrum was taken at an edge region in contrast to the first two spectra that were taken at the center region.[59–61] During the preparation of the source sample, some excess silver nitrate from the supernatant could have become entrained in the precipitate. During the evaporation step, the silver nitrate could have also migrated towards the edges, causing a higher silver content around the precipitate edges. Therefore, Spectra 1 and 2 are a better representation of the majority of the precipitate.[62]

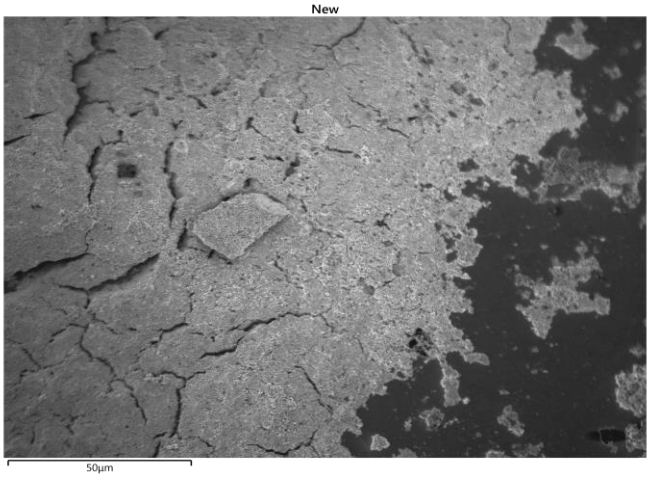

(a)

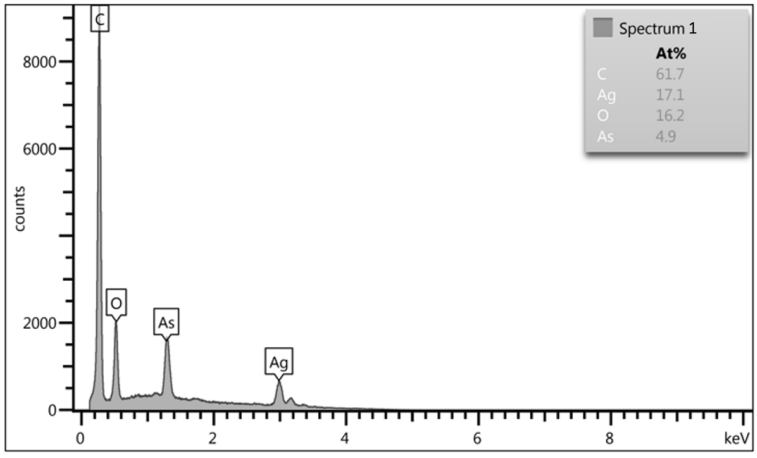

(b)

Figure 12: (a) SEM image of the stable arsenic precipitate. (b) EDS spectrum of the stable arsenic precipitate taken from a point (Spectrum 1) in the shown SEM image.

Table 7: Atomic percentages of the detected elements from each spectrum, and the calculated ratio of each element for the precipitate.

ID	Ag (atomic %)	As (atomic %)	O (atomic %)	C (atomic %)	Predicted Ratio (Ag:As:O)
Spectrum 1	17.1	4.9	16.2	61.7	3.5:1:3.3
Spectrum 2	15.8	4.9	12.6	66.7	3.2:1:2.6
Spectrum 3	36.6	3.8	57.5	2.1	9.6:1:15.0

3.13: XPS Analysis

X-Ray Photoelectron Spectroscopy (XPS) was also performed on the stable arsenic sample, as depicted in Table 8, revealing the presence of the same elements observed in the SEM-EDS measurements. The quantities of silver, arsenic, and oxygen are also comparable with the SEM-EDS results. Furthermore, the detection of carbon on the precipitate was similarly confirmed via XPS. The small amount of nitrogen identified could potentially be attributed to a stray peak from another element noted in the spectrum.

The enlarged portion of the XPS spectrum, illustrated in Figure 13, can be attributed to the peak arising from the As-O bond. The spectrum was fitted to illustrate the contributions of As-O bonds in the As(III) and As(V) compounds to the As $3d_{5/2}$ peak. Literature indicates that the As $3d_{5/2}$ position for oxygen-containing compounds of As(III) falls within the range of 44.7 – 45.1eV, while for As(V) counterparts, it typically ranges slightly higher, between 45.8 – 46.2eV.[63] The fitted spectrum suggests that the arsenic-based precipitate comprises a combination of As(III) and As(V), with proportions of 78.3% and 21.7%, respectively. During the initial step of sample preparation, arsenic was fully converted from the +3 to +5 oxidation state and the majority of As in the precipitate was expected to be present as arsenic (V). Literature suggests the X-ray-induced photo-reduction of arsenic oxides could be a potential influence factor on this measurement, translating to the reduction of arsenic (V) species to arsenic (III). This reduction is magnified depending on the intensity of the X-rays and the presence of carbon. X-ray irradiation on hydrocarbons can induce the formation of highly energetic radicals that can strip oxygen from the arsenic oxide surface, further reducing it to arsenic (III).[64] The addition of hexane rinses introduced an excess of carbon to the source sample, thereby promoting the probability for the reduction of arsenic. Therefore, using XPS to determine the oxidation state of As in this sample, which could point towards a specific silver-arsenic compound, showed to be of limited

significance.

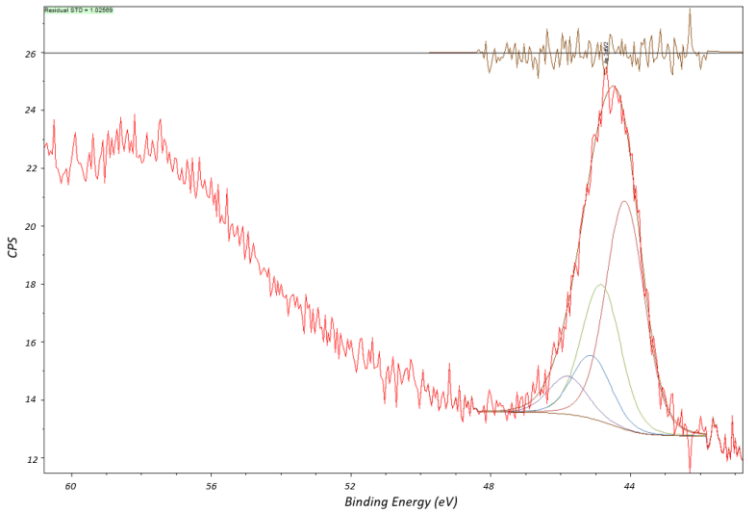

Figure 13: Arsenic spectrum obtained from XPS.

Table 8: Data table of all detected elements from the stable arsenic sample, along with their percent compositions.

ID	Composition (Atomic %)
C	33.75
O	32.3
Ta	5.45
As	8.0
Ag	18.0
N	2.5

However, considering the composition of the precipitate estimated via XPS, together with the results from the SEM-EDS analysis and the ICP-OES data from the supernatant, it can be deduced that a compound containing Ag, As, and O at a stoichiometric ratio that points towards silver arsenate or silver arsenite was produced. Furthermore, both SEM-EDS and XPS findings highlight the presence of carbon, indicating that in subsequent source sample preparations, the use of hexane rinses should be avoided.

3.14: ^{73}As Beam Delivery

The fabricated ^{73}As source sample was introduced into BMIS, where the ^{73}As was extracted as a monovalent ion, $^{73}As^{+}$, with a mass of 73. Scientific users utilized the resulting ^{73}As

beam to investigate the reaction $^{73}As(p,\gamma)^{74}Se$, crucial for the production of ^{74}Se in stellar environments.[65] Figure 14 illustrates the mass scans of the relevant region obtained from a stable silver arsenate sample, depicting stable silver and arsenic species at masses 107, 109, and 75, respectively. This source sample was employed for the development of the beam extraction and beam delivery. However, the mass scan for the radioactive ^{73}As source sample was similar, only showing the stable species, while the low-level ^{73}As signal at mass 73 would remain indiscernible. Such behavior is anticipated for a low-mass sample; nonetheless, mass 73 was selected by the mass analyzer, and the ion beam was accelerated and delivered at an average rate of $5*10^5$ particles per second to the ReAccelerator, achieving beam impurities close to 100%. However, to attain sufficient beam rates, the oven temperature needed to be elevated to approximately 870ºC. This observation aligns with the reported melting point of silver arsenate, noted at 830ºC. The two peaks observed at masses 107 and 109 originate from the two naturally occurring silver isotopes: ^{107}Ag (51.839%) and ^{109}Ag (48.161%).[50] The observed strong signal can be attributed to the nine-fold excess of silver used to initiate the precipitation reaction.

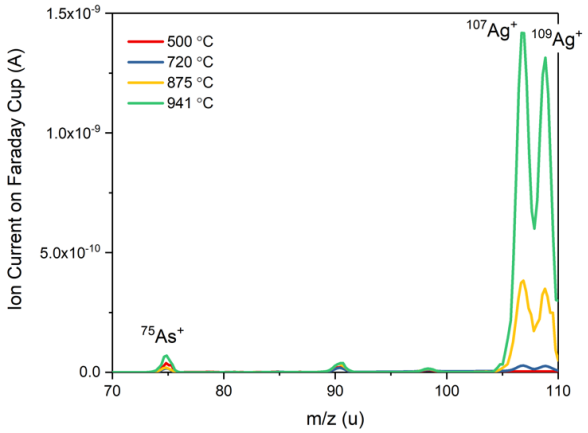

Figure 14: Mass scans of introduced stable source sample of ^{75}As, alongside the co-present stable silver isotopes, ^{107}Ag and ^{109}Ag, at oven temperatures ranging from 500ºC to 941ºC.

After the ^{73}As beam was extracted from BMIS, it was sent to the ReAccelerator, where the beam was accelerated to the desired low energy requested by the scientific users. Figure 15 shows the measurement of ^{73}As on a silicon detector, where the strong signal at 356MeV translates to a beam energy of 4.88MeV/u that matches with the expected beam energy for ^{73}As, thereby serving as a means of identification.

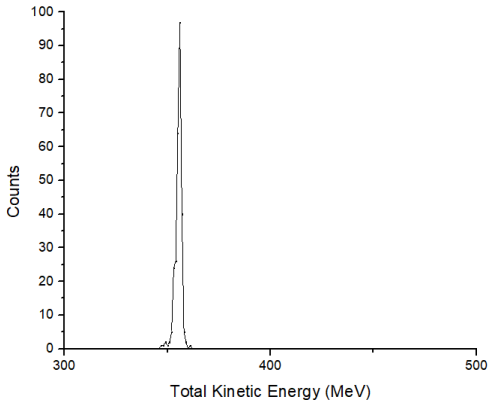

Figure 15: Spectrum of the ^{73}As beam after passing through the ReAccelerator.

3.15: Conclusions

This study demonstrates the preparation of a ^{73}As source sample utilized in the offline ion source BMIS to generate a ^{73}As beam, facilitating the low-energy scientific user program at FRIB. Silver arsenate, chosen for its favorable volatility within the operating temperature range of BMIS, was synthesized via chemical precipitation, yielding high precipitation yields (99.4%) with the ^{73}As sample. The prepared ^{73}As source sample (1.556mCi, $5.76*10^{14}$ atoms ^{73}As) was utilized to successfully deliver a pure $^{73}As^{+}$ ion beam at a suitable rate for an eight-day-long user experiment. Characterization via SEM-EDS and XPS revealed a silver arsenic compound, though determining exact stoichiometry proved challenging. Several improvements for refining the source sample manufacturing process were identified, such as avoiding the use of hexane and enhancing the quantitative transfer of ^{73}As activity through the use of nitric acid. This developed preparation method expands the array of low-energy and stopped ion beams for FRIB's offline beam program, particularly enriching nuclear sciences with the inclusion of the ^{73}As beam.

3.16: ^{232}Th Source Samples Preparation and Analysis of $ThCl_4$

After preparation of the ^{73}As source sample, the BMIS team had interest in developing a ^{232}Th beam, which would serve as a surrogate for a ^{229}Th beam requested by scientific users. This would be the first heavy element beam that would be generated from BMIS. For this initial experiment, about 5mL of ICP standard solution, containing 1000 ± 10ppm thorium in 5% HNO_3 (GFS Chemicals), was first precipitated as thorium hydroxide by the addition of ammonium hydroxide (reaction 4), followed by the dissolution in hydrochloric acid to form thorium chloride (reaction 5).[66,67]

$$Th(NO_3)_4(aq) + 4NH_4OH(aq) \rightarrow Th(OH)_4(s) + 4NH_4NO_3(aq) \quad (4)$$

$$Th(OH)_4(s) + 4HCl(aq) \rightarrow ThCl_4(aq) + 4H_2O \quad (5)$$

Thorium chloride was chosen as its melting point is 770ºC, which falls within the operating temperature range of BMIS.[68] The BMIS team intended to utilize a source sample of 500µg thorium chloride for their initial test run. A small volume of the thorium ICP standard was brought to a residue and reconstituted in MilliQ water, following the stock preparation procedure outlined in section 2.2.2. After the stock preparation, 1M ammonium hydroxide was added until no more visible precipitation formed. The mixture was centrifuged and rinsed several times to remove any nitrate impurities. The thorium hydroxide was dissolved using 37% HCl and transferred onto a sheet of tantalum foil, similar to the source sample preparation described in section 3.2.5.

After inserting the prepared source sample into BMIS, it was exceedingly challenging to extract a thorium beam. A possible reaction might be that the thorium chloride transformed into highly refractory thorium oxide in the high-temperature environment of BMIS. This is further corroborated by the observation that the prepared thorium source sample started to adsorb water immediately after it was removed from the hot plate. SEM-EDS was done and could support those presumptions; Table 9 from each spectra indicates that some oxygen is also present. It is possible that under atmospheric conditions, the thorium chloride adsorbs the moisture from the air due to its hygroscopic nature.[69] In the BMIS environment, the entrained water in the source samples forms the highly refractory thorium oxide. The exceedingly high melting point of thorium oxide (3350ºC) would explain the small extracted beam current, as this temperature is well above the operating temperature range of BMIS.[68] Further investigation is necessary to develop a suitable thorium source sample.

Table 9: SEM-EDS data of all the spectra taken from the thorium sample, alongside the percentage of thorium, chlorine, and oxygen present in the sample.

Spectrum #	Th (%)	Cl (%)	O (%)
1	61.7	29.0	9.3
2	62.9	28.5	8.6
3	63.0	27.2	9.8
4	61.1	29.4	9.4

3.17: Conclusions

A preliminary ^{232}Th source sample was prepared, which was the first test extraction of a heavy element from the BMIS. Sample preparation was done by precipitation as thorium

hydroxide, and dissolution in hydrochloric acid to yield thorium chloride. Through SEM-EDS, the presence of thorium, chlorine, and some oxygen was corroborated. The initial run in the BMIS and the results of the SEM-EDS analysis support that due to the hygroscopic nature of the thorium chloride, a highly refractory compound formed. Further research into different targetry options and beam extraction are required to extract thorium beams at the required higher currents.

CHAPTER 4: Conclusion

The work herein outlined in this dissertation aimed to further advance the endeavors in the proposed methodology for isotope harvesting endeavors at FRIB. The goals were to demonstrate the potential for metal oxides as a sorbent for aqueous isotope harvesting. These materials are interesting, as they would allow a direct combination with a subsequent mass-separation step that is necessary to produce samples of high radioisotopic purity. The sorption abilities of seven commercially available metal oxides were evaluated towards 10 stable elements that represent the interesting Ni isotopes, as well as the other primarily formed isotopes. Magnesium oxide demonstrated promising sorbent properties for all tested species, though it is partially water-soluble and strongly altered the pH of the water solution, thereby introducing ions into the water. Nevertheless, a magnesium oxide sample with adsorbed stable ^{61}Ni was prepared and the extraction of a ^{61}Ni beam from this support material was tested in the BMIS. The extraction of ^{61}Ni from the oxide matrix proved exceedingly difficult, in part due to the formation of highly refractory species. Compounded by adsorption results that did not meet our requirements, it was decided to disconnect the mass-separation step and isotope harvesting. This offers additional advantages of implementing a chemical pre-separation to produce cleaner samples and also offers more flexibility for tailoring the targetry for mass separation. However, the adsorption of specific elements on certain, water-insoluble metal oxides, like silicon dioxide, could be considered for specific harvesting applications in the future.

Furthermore, the collaboration with the BMIS team also extended towards the preparation of source samples to generate low-energy and stopped beams for the FRIB user program. Through this work, further insight into the operation and requirements of samples for mass separation could be gained. The first effort involved developing a ^{73}As source sample. The ^{73}As source was prepared through precipitation into silver arsenate. Sample characterization through SEM-EDS and XPS of the stable silver arsenate confirmed the elements present and that a silver-arsenic precipitate did form, though the exact species of arsenic that formed was not readily determined. After preparation of the ^{73}As source sample, the BMIS team was able to deliver a ^{73}As beam that was employed by scientific users to gain insights into the astro-physically significant ^{73}As(p,γ)^{74}Se reaction. The outcome of the sample sample preparation work is intended for publication as a Short Communication paper in the Journal of Applied Radiation & Isotopes.

BIBLIOGRAPHY

(1) Cadman, L. *MEETING ISOTOPE NEEDS AND CAPTURING OPPORTUNITIES FOR THE FUTURE: The 2015 Long Range Plan for the DOE-NP Isotope Program*; 2015.

(2) *Radiation Facts Radiation and Airport Security Scanning*. https://www.epa.gov/radtown/radiation-and-airport-security-scanning.

(3) *List of Nickel Isotopes and Nickel Applications*. https://www.buyisotope.com/nickel-isotopes.php.

(4) Matarrese, M.; Bedeschi, P.; Scardaoni, R.; Sudati, F.; Savi, A.; Pepe, A.; Masiello, V.; Todde, S.; Gianolli, L.; Messa, C.; Fazio, F. Automated Production of Copper Radioisotopes and Preparation of High Specific Activity [64Cu]Cu-ATSM for PET Studies. *Applied Radiation and Isotopes* **2010**, *68* (1), 5–13. https://doi.org/10.1016/j.apradiso.2009.08.010.

(5) Rehm, K. E.; Borasi, F.; Jiang, C. L.; Ackermann, D.; Ahmad, I.; Brumwell, F.; Davids, C. N.; Decrock, P.; Fischer, S. M.; Gok, J.; Greene, J. P.; Hackmann, G.; Harss, B.; Henderson, D.; Henning, W.; Janssens, R. V. F.; Mcmichael, G.; Nanal, V.; Nisius, D.; Nolen, J.; Pardo, R. C.; Paul, M.; Reiter, P.; Schi, J. P.; Er, !; Seweryniak, D.; Segel, R. E.; Wiedenhok, I.; Wiescher, M.; Wuosmaa, A. H. *Experiments with a Radioactive 56Ni Beam*; 2000; Vol. 449.

(6) Suryanto, H.; Kambali, I. A Novel Method for 57Ni and 57Co Production Using Cyclotron-Generated Secondary Neutrons. *Atom Indonesia* **2018**, *44* (2), 81–87. https://doi.org/10.17146/aij.2018.872.

(7) Nielsen, G. D.; Andersen, O.; Jensen, M. Toxicokinetics of Nickel in Mice Studied with the γ-Emitting Isotope 57Ni. *Fundamental and Applied Toxicology* **1993**.

(8) Mcaninch, J. E.; Hainsworth, L. J.; Marchetti, A. A.; Leivers, M. R.; Jones, P. R.; Dunlop, A. E.; Mauthe, R.; Vogel, J. S.; Proctor, I. D.; Straume, T. *Measurement of 63Ni and 59Ni by Accelerator Mass Spectrometry Using Characteristic Projectile X-Rays*; 1997; Vol. 123.

(9) Radiation Safety Data - 63Ni Electron Capture Detectors.

(10) Making Radioactive 63Ni to Target Explosives. **2011**.

(11) Paul, M.; Fifield, L. K.; Fink, D.; Albrecht, A.; Allan, G. L.; Herzog, G.; Tuniz, C. Measurements of 59Ni in Meteorites by Accelerator Mass Spectrometry. *Nuclear Instruments and Methods in Physics Research* **1993**.

(12) Weiss, C.; Guerrero, C.; Griesmayer, E.; Adrzejewski, J.; Badurek, G.; Chiaveri, E.; Dressler, R.; Ganesan, S.; Jericha, E.; Kaeppeler, F.; Koehler, P.; Lederer, C.; Leeb, H.; Marganiec, J.; Pavlik, A.; Perkowski, J.; Reifarth, R.; Rauscher, T.; Schumann, D.; Tagliente, G.; Vlachoudis, V. The (n, α) Reaction in the s-Process Branching Point 59Ni.

2012.

(13) Gopalakrishnan, V.; Nandedkar, R. V; Ganesan, S. *Comparison of Calculated Helium Production in Stainless Steel Due to Neutron Irradiation with Experiment*; 1996; Vol. 228.

(14) *Handbook of Nuclear Chemistry*.

(15) Ahmadi-Motlagh, M.; Amini, Y.; Karimi-Sabet, J. Experimental Study of Nitrogen Isotope Separation by Ion-Exchange Chromatography: Effect of Process Factors. *J Radioanal Nucl Chem* **2022**, *331* (1), 309–315. https://doi.org/10.1007/s10967-021-08079-y.

(16) Gade, A.; Sherrill, B. M. *NSCL and FRIB at Michigan State University: Nuclear Science at the limits of Stability*; 2016.

(17) Wei, J. *Progress Towards the Facility for Rare Isotope Beams*; 2013.

(18) Abel, E. P.; Domnanich, K.; Kalman, C.; Walker, W.; Engle, J. W.; Barnhart, T. E.; Severin, G. Durability Test of a Flowing-Water Target for Isotope Harvesting. *Nucl Instrum Methods Phys Res B* **2020**, *478*, 34–45. https://doi.org/10.1016/j.nimb.2020.05.011.

(19) Loveless, C. S.; Marois, B. E.; Ferran, S. J.; Wilkinson, J. T.; Sutherlin, L.; Severin, G.; Shusterman, J. A.; Scielzo, N. D.; Stoyer, M. A.; Morrissey, D. J.; Robertson, J. D.; Peaslee, G. F.; Lapi, S. E. Harvesting 48V at the National Superconducting Cyclotron Laboratory. *Applied Radiation and Isotopes* **2020**, *157*. https://doi.org/10.1016/j.apradiso.2019.109023.

(20) Mastren, T.; Pen, A.; Peaslee, G. F.; Wozniak, N.; Loveless, S.; Essenmacher, S.; Sobotka, L. G.; Morrissey, D. J.; Lapi, S. E. Feasibility of Isotope Harvesting at a Projectile Fragmentation Facility: 67Cu. *Sci Rep* **2014**, *4*. https://doi.org/10.1038/srep06706.

(21) Abel, E. P.; Domnanich, K.; Clause, H. K.; Kalman, C.; Walker, W.; Shusterman, J. A.; Greene, J.; Gott, M.; Severin, G. W. Production, Collection, and Purification of 47Ca for the Generation of 47Sc through Isotope Harvesting at the National Superconducting Cyclotron Laboratory. *ACS Omega* **2020**, *5* (43), 27864–27872. https://doi.org/10.1021/acsomega.0c03020.

(22) Clause, H. K.; Domnanich, K. A.; Kleinfeldt, C.; Kalman, M.; Walker, W.; Vyas, C.; Abel, E. P.; Severin, G. W. Harvesting Krypton Isotopes from the Off-Gas of an Irradiated Water Target to Generate 76Br and 77Br. *Sci Rep* **2022**, *12* (1). https://doi.org/10.1038/s41598-022-05500-8.

(23) Domnanich, K. A.; Vyas, C. K.; Abel, E. P.; Kalman, C.; Walker, W.; Severin, G. W. Harvesting 62Zn from an Aqueous Cocktail at the NSCL. *New Journal of Chemistry* **2020**, *44* (47), 20861–20870. https://doi.org/10.1039/d0nj04411c.

(24) Abel, E. P.; Clause, H. K.; Severin, G. W. Radiolysis and Radionuclide Production in a

Flowing-Water Target during Fast 40Ca20+ Irradiation. *Applied Radiation and Isotopes* **2020**, *158*. https://doi.org/10.1016/j.apradiso.2020.109049.

(25) Mastren, T.; Pen, A.; Loveless, S.; Marquez, B. V.; Bollinger, E.; Marois, B.; Hubley, N.; Brown, K.; Morrissey, D. J.; Peaslee, G. F.; Lapi, S. E. Harvesting 67Cu from the Collection of a Secondary Beam Cocktail at the National Superconducting Cyclotron Laboratory. *Anal Chem* **2015**, *87* (20), 10323–10329. https://doi.org/10.1021/acs.analchem.5b02322.

(26) Pen, A.; Mastren, T.; Peaslee, G. F.; Petrasky, K.; Deyoung, P. A.; Morrissey, D. J.; Lapi, S. E. Design and Construction of a Water Target System for Harvesting Radioisotopes at the National Superconducting Cyclotron Laboratory. *Nucl Instrum Methods Phys Res A* **2014**, *747*, 62–68. https://doi.org/10.1016/j.nima.2014.02.010.

(27) Domnanich, K. A.; Satija, S.; Bodnar, V. S.; Bollen, G.; Kleinfeldt, C. R.; Liu, Y.; Rogers, S.; Schwarz, S.; Severin, G. W.; Sumithrarachchi, C.; Villari, A. C. C. Preparation of Stable and Long-Lived Source Samples for the Stand-Alone Beam Program at the Facility for Rare Isotope Beams. *Applied Radiation and Isotopes* **2023**, *200*. https://doi.org/10.1016/j.apradiso.2023.110958.

(28) Sumithrarachchi, C. S.; Liu, Y.; Rogers, S. N.; Schwarz, S.; Bollen, G.; Gamage, N.; Henriques, A.; Lapierre, A.; Ringle, R.; Yandow, I.; Villari, A. C. C.; Domnanich, K. A.; Satija, S.; Severin, G. W.; Au, M.; Ballof, J.; Garcia, Y. N. V.; Owen, M.; Reis, E.; Rothe, S.; Stegemann, S. The New Batch Mode Ion Source for Stand-Alone Operation at the Facility for Rare Isotope Beams (FRIB). *Nucl Instrum Methods Phys Res B* **2023**, *541*, 301–304. https://doi.org/10.1016/j.nimb.2023.05.061.

(29) Köster, U. *ISOLDE Target and Ion Source Chemistry*; 2001; Vol. 89.

(30) Duchemin, C.; Ramos, J. P.; Stora, T.; Ahmed, E.; Aubert, E.; Audouin, N.; Barbero, E.; Barozier, V.; Bernardes, A. P.; Bertreix, P.; Boscher, A.; Bruchertseifer, F.; Catherall, R.; Chevallay, E.; Christodoulou, P.; Chrysalidis, K.; Cocolios, T. E.; Comte, J.; Crepieux, B.; Deschamps, M.; Dockx, K.; Dorsival, A.; Fedosseev, V. N.; Fernier, P.; Formento-Cavaier, R.; El Idrissi, S.; Ivanov, P.; Gadelshin, V. M.; Gilardoni, S.; Grenard, J. L.; Haddad, F.; Heinke, R.; Juif, B.; Khalid, U.; Khan, M.; Köster, U.; Lambert, L.; Lilli, G.; Lunghi, G.; Marsh, B. A.; Palenzuela, Y. M.; Martins, R.; Marzari, S.; Menaa, N.; Michel, N.; Munos, M.; Pozzi, F.; Riccardi, F.; Riegert, J.; Riggaz, N.; Rinchet, J. Y.; Rothe, S.; Russell, B.; Saury, C.; Schneider, T.; Stegemann, S.; Talip, Z.; Theis, C.; Thiboud, J.; van der Meulen, N. P.; van Stenis, M.; Vincke, H.; Vollaire, J.; Vuong, N. T.; Webster, B.; Wendt, K.; Wilkins, S. G. CERN-MEDICIS: A Review Since Commissioning in 2017. *Front Med (Lausanne)* **2021**, *8*. https://doi.org/10.3389/fmed.2021.693682.

(31) Ješkovský, M.; Kaizer, J.; Kontuí, I.; Lujanienė, G.; Müllerová, M.; Povinec, P. P. Analysis of Environmental Radionuclides. In *Handbook of Radioactivity Analysis: Volume 2: Radioanalytical Applications*; Elsevier, 2020; pp 137–261. https://doi.org/10.1016/B978-0-12-814395-7.00003-9.

(32) Köster, U.; Carbonez, P.; Dorsival, A.; Dvorak, J.; Eichler, R.; Fernandes, S.; Frånberg,

H.; Neuhausen, J.; Novackova, Z.; Wilfinger, R.; Yakushev, A. (Im-)Possible ISOL Beams. In *European Physical Journal: Special Topics*; 2007; Vol. 150, pp 285–291. https://doi.org/10.1140/epjst/e2007-00326-1.

(33) El-Samak, A. A.; Rahman, H.; Ponnamma, D.; Hassan, M. K.; Zaidi, S. J.; Al-Maadeed, M. A. A. Role of Metal Oxide Nanofibers in Water Purification. In *Metal Oxide-Based Nanofibers and Their Applications*; Elsevier, 2021; pp 173–190. https://doi.org/10.1016/B978-0-12-820629-4.00001-1.

(34) Schoonen, M. A. A. *Calculation of the Point of Zero Charge of Metal Oxides between 0 and 350°C*; 1994; Vol. 58.

(35) Ibanez, J.; Hernandez-Esparza, M.; Doria-Serrano, C.; Fregoso-Infante, A.; Singh, M. *Environmental Chemistry*; 2008.

(36) Payus, C. M.; Jikilim, C.; Sentian, J. Rainwater Chemistry of Acid Precipitation Occurrences Due to Long-Range Transboundary Haze Pollution and Prolonged Drought Events during Southwest Monsoon Season: Climate Change Driven. *Heliyon* **2020**, *6* (9). https://doi.org/10.1016/j.heliyon.2020.e04997.

(37) Ocean Acidification. **2020**.

(38) Holder, C. F.; Schaak, R. E. Tutorial on Powder X-Ray Diffraction for Characterizing Nanoscale Materials. *ACS Nano*. American Chemical Society July 23, 2019, pp 7359–7365. https://doi.org/10.1021/acsnano.9b05157.

(39) Rowe, M. C.; Brewer, B. J. AMORPH: A Statistical Program for Characterizing Amorphous Materials by X-Ray Diffraction. *Comput Geosci* **2018**, *120*, 21–31. https://doi.org/10.1016/j.cageo.2018.07.004.

(40) Dyamond, S. *The Role of Background Electrolyte on Metal Ion Adsorption*; 2023.

(41) Kosmulski, M. Isoelectric Points and Points of Zero Charge of Metal (Hydr)Oxides: 50 Years after Parks' Review. *Advances in Colloid and Interface Science*. Elsevier B.V. December 1, 2016, pp 1–61. https://doi.org/10.1016/j.cis.2016.10.005.

(42) Brown, S. A.; Brown, P. L. The PH-Potential Diagram for Polonium. In *The Aqueous Chemistry of Polonium and the Practical Application of its Thermochemistry*; Elsevier, 2020; pp 121–126. https://doi.org/10.1016/b978-0-12-819308-2.00004-8.

(43) *Atlas of Eh-PH Diagrams Intercomparison of Thermodynamic Databases*; 2005.

(44) Railsback. Characterization of Solutions by PH and Eh. *Some Fundamentals of Mineralogy and Geochemistry* **2006**.

(45) *Exploring Le Chatelier's Principle: What Factors Control the Equilibrium of Cobalt Complex Ions? 1*.

(46) Chang, Q. Surface of Solids. In *Colloid and Interface Chemistry for Water Quality*

Control; Elsevier, 2016; pp 175–225. https://doi.org/10.1016/b978-0-12-809315-3.00010-4.

(47) Suresh Kumar, P.; Korving, L.; Keesman, K. J.; van Loosdrecht, M. C. M.; Witkamp, G. J. Effect of Pore Size Distribution and Particle Size of Porous Metal Oxides on Phosphate Adsorption Capacity and Kinetics. *Chemical Engineering Journal* **2019**, *358*, 160–169. https://doi.org/10.1016/j.cej.2018.09.202.

(48) Tewari, P. H.; Campbell, A. B.; Lee, W. *Adsorption of Co2+ by Oxides from Aqueous Solution*; 1972; Vol. 50.

(49) Sherrill, B. M. Future Opportunities at the Facility for Rare Isotope Beams. In *EPJ Web of Conferences*; EDP Sciences, 2018; Vol. 178. https://doi.org/10.1051/epjconf/201817801001.

(50) *Live-Chart of Nuclides*. https://www-nds.iaea.org/relnsd/vcharthtml/VChartHTML.html.

(51) Gyürky, G.; Fülöp, Z.; Käppeler, F.; Kiss, G. G.; Wallner, A. The Activation Method for Cross Section Measurements in Nuclear Astrophysics. *European Physical Journal A*. Springer New York LLC March 1, 2019. https://doi.org/10.1140/epja/i2019-12708-4.

(52) Nichols, A. L. *Comments on Evaluation 73 Se Se-Comments on Evaluation of Decay Data*; 2014.

(53) Minamisono, K.; Mantica, P. F.; Klose, A.; Vinnikova, S.; Schneider, A.; Johnson, B.; Barquest, B. R. Commissioning of the Collinear Laser Spectroscopy System in the BECOLA Facility at NSCL. *Nucl Instrum Methods Phys Res A* **2013**, *709*, 85–94. https://doi.org/10.1016/j.nima.2013.01.038.

(54) Villari, A. C. C.; Arend, B.; Bollen, G.; Crisp, D. B.; Davidson, K. D.; Fukushima, K.; Henriques, A. I.; Holland, K.; Kim, S.-H.; Lapierre, A.; Liu, Y.; Maruta, T.; Morris, D. G.; Morrissey, D. J.; Nash, S.; Ostroumov, P. N.; Plastun, A. S.; Priller, J.; Schwarz, S.; Sherrill, B. M.; Steiner, M.; Sumithrarachchi, C.; Walker, R.; Zhang, T.; Zhao, Q. UPGRADE OF THE FRIB ReACCELERATOR*. **2022**. https://doi.org/10.18429/JACoW-NAPAC2022-WEYE2.

(55) Udovit Molmir, L. ’; Vir~ikova, E.; Lech, P. *Experimental Study of As (III) Oxidation by Hydrogen Peroxide*; 1994.

(56) Curtman, L. J.; Daschavsky, P.; J Curtman, B. L. *A Study of the Silver Arsenate Test for Arsenic*; 1916. https://pubs.acs.org/sharingguidelines.

(57) Smedley, P. L.; Kinniburgh, D. G. *A Review of the Source, Behaviour and Distribution of Arsenic in Natural Waters*; 2001. www.elsevier.com/locate/apgeochem.

(58) *Properties of Substance: Silver Arsenate*.

(59) Goldstein, J. I.; Newbury, D. E.; Echlin, P.; Joy, D. C.; Lyman, C. E.; Lifshin, E.; Sawyer, L.; Michael, J. R. *Scanning Electron Microscopy and X-Ray Microanalysis*; Springer US:

Boston, MA, 2003. https://doi.org/10.1007/978-1-4615-0215-9.

(60) Duma, Z. S.; Sihvonen, T.; Havukainen, J.; Reinikainen, V.; Reinikainen, S. P. Optimizing Energy Dispersive X-Ray Spectroscopy (EDS) Image Fusion to Scanning Electron Microscopy (SEM) Images. *Micron* **2022**, *163*. https://doi.org/10.1016/j.micron.2022.103361.

(61) Byrne, R. G.; McGladdery, R. J.; Zhou, Z.; Thomson, R. C.; Doak, S. S.; Jepson, M. A. E. Detection and Quantification of Precipitates in 11–12 Wt% Cr Steels Using in-Column Secondary Electron Detectors. *Mater Charact* **2020**, *165*. https://doi.org/10.1016/j.matchar.2020.110356.

(62) Cristea-Stan, D.; Mereuta, P.; Constantinescu, B.; Ceccato, D. *ANCIENT SILVER AND BRONZE METALLURGY STUDIES BY MICRO-PIXE AND SEM-EDS*; 2018.

(63) Moulder, J. F.; Chastain, Jill. *Handbook of X-Ray Photoelectron Spectroscopy : A Reference Book of Standard Spectra for Identification and Interpretation of XPS Data*; Physical Electronics Division, Perkin-Elmer Corp, 1992.

(64) Viltres, H.; Odio, O. F.; Lartundo-Rojas, L.; Reguera, E. Degradation Study of Arsenic Oxides under XPS Measurements. *Appl Surf Sci* **2020**, *511*. https://doi.org/10.1016/j.apsusc.2020.145606.

(65) Kusakabe, M.; Iwamoto, N.; Nomoto, K. Production of the P-Process Nuclei in the Carbon-Deflagration Model for Type Ia Supernovae. *Astrophysical Journal* **2011**, *726* (1). https://doi.org/10.1088/0004-637X/726/1/25.

(66) Sukarsono, D. R.; Masduki, B.; Suryawan, I. MEMPELAJARI PENGENDAPAN CAMPURAN TORIUM HIDROKSIDA DAN AMMONIUM DIURANAT. **1996**.

(67) Morss, L. R.; Edelstein, N. M.; Fuger, J. *The Chemistry of the Actinide and Transactinide Elements - Third Edition*; 2006.

(68) Haynes, W. M. *Handbook of Chemistry and Physics - 95th Edition*; 2015.

(69) Dock, C. H. *Oxidation States of Thorium in Fused LiCl-Kcl EUTECTIC*; Ames, 1965.